ERK phosphorylation is RAF-independent in naïve and activated B cells but RAF-dependent in plasma cell differentiation

Laura Scheffler[1#], Samantha Feicht[1,2#], Tea Babushku[1], Laura B. Kuhn[1], Stefanie Ehrenberg[1], Samantha Frankenberger[1], Frank M. Lehmann[2,3], Elias Hobeika[4,5], Berit Jungnickel[2,6], Manuela Baccarini[7], Georg W. Bornkamm[2, 8], Lothar J. Strobl[1], Ursula Zimber-Strobl[1*]

[1] Research Unit of Gene Vectors, Helmholtz Center Munich, German Research Center for Environmental Health GmbH, Marchioninistrasse 25, D-81377 Munich, Germany.
[2] Institute for Clinical Molecular Biology and Tumor Genetics, Helmholtz Center Munich, German Research Center for Environmental Health GmbH, Marchioninistrasse 25, D-81377 Munich, Germany.
[3] present address: Department of Biomedicine and University Children's Hospital of Basel, University of Basel, 4058 Basel, Switzerland
[4] Molecular Immunology, Max Planck Institute of Immunobiology and Epigenetics, Stübeweg 51, D-79108 Freiburg, Germany.
[5] Institute of Immunology, Ulm University Medical Center, Albert-Einstein-Allee 11, D-89070 Ulm, Germany.
[6] Department of Cell Biology, Institute of Biochemistry and Biophysics, Center for Molecular Biomedicine, Friedrich-Schiller University Jena, Hans-Knoell-Strasse 2, D-07745 Jena, Germany.
[7] Department of Microbiology, Immunobiology and Genetics, Center for Molecular Biology of the University of Vienna, Max Perutz Labs, Dr. Bohr-Gasse 9, 1030 Vienna, Austria.
[8] present address: Institute of Experimental Cancer Research, University of Ulm, Albert-Einstein-Allee 11, D-89081 Ulm, Germany
[#] These authors contributed equally.

* Corresponding author. E-mail: strobl@helmholtz-muenchen.de

Abstract

Members of the RAF family of serine-threonine kinases are intermediates in the mitogen-activated protein kinase and extracellular signal–regulated kinase (MAPK-ERK) signaling pathway, which controls key differentiation processes in B cells. By analyzing mice with B cell–specific deletion of *Raf1*, *Braf*, or both, we showed that Raf-1 and B-Raf acted together in mediating the positive selection of pre-B and transitional B cells as well as in initiating plasma cell (PC) differentiation. Unexpectedly, genetic or chemical inactivation of RAFs led to increased amounts of ERK phosphorylation in mature B cells. ERK activation in the absence of Raf-1 and B-Raf was mediated not by A-Raf, the third member of the RAF family member in mammals, but by multiple RAF-independent pathways, with phosphoinositide 3-kinase (PI3K) playing an important role. Furthermore, we found that ERK phosphorylation strongly increased during the transition from activated B cells to pre-plasmablasts. This increase in ERK phosphorylation was not achieved in B cells lacking both Raf-1 and B-Raf, and most likely explains the partial block of PC differentiation in animals lacking both RAFs. Collectively, our data indicate that B-Raf and Raf-1 are not necessary to mediate ERK phosphorylation in naïve and activated B cells but are essential for mediating the sharp increase in ERK phosphorylation during the transition from activated B cells to pre-plasmablasts.

Introduction

The RAF family of serine-threonine kinases in mammals consists of RAF-1 (also known as C-RAF), B-RAF and A-RAF. These kinases are involved in the activation of the mitogen-activated protein kinase kinase–extracellular signal–regulated kinase (MEK/ERK) signaling pathway downstream of several receptors, including tyrosine kinase receptors and members of the tumor-necrosis factor receptor (TNF-R) family. Activation of the kinase ERK occurs in most cases through a signaling cascade of sequential phosphorylation events through RAS-RAF-MEK-ERK (*1*). It is well established that ERK is activated downstream of the B cell receptor (BCR), but details about the role of RAF kinases in the activation of MEK/ERK in mammalian B lymphocytes are unclear.

In mammals, B cell development takes place in the bone marrow (BM), where B cells develop from pro- to pre- and, finally, immature B cells. These cells leave the BM and migrate to the spleen where they develop further through the transitional stages type 1 (T1) and type 2 (T2) to give rise to either follicular B (Fo B) cells or marginal zone B (MZ B) cells (*2, 3*). Both RAS and ERK have been suggested to control important checkpoints during B cell development downstream of the pre-BCR and BCR, ensuring the generation of B cells expressing a functional but not autoreactive B cell receptor (*4-10*).

In the periphery, mature B cells can be activated to perform either T cell–independent (TI) or T cell–dependent (TD) immune responses. B1a and MZ B cells respond mainly to TI antigens by rapidly differentiating into plasma cells (PCs) that secrete low-affinity antibodies. In contrast, Fo B cells react to TD antigens and, along with T cells, form germinal centers (GC), in which high-affinity PC and memory B cells are generated. Ablation of ERK1 and ERK2 in GC B cells profoundly

compromises PC differentiation, suggesting that ERKs are essential for PC differentiation (*11*). However, whether RAFs also contribute to PC differentiation by mediating the phosphorylation of ERK has not been investigated in this context. To study the role of B-Raf and Raf-1 in B cell development and activation, we inactivated *Braf* and *Raf1* alone and in combination specifically in B cells. We demonstrated that Raf-1 and B-Raf acted together in controlling the positive selection of pre-B and transitional B cells. Moreover, we found that Raf-1 and B-Raf were not necessary to mediate phosphorylation of ERK in mature and activated B cells but rather attenuated the amount of phosphorylated ERK (pERK) in these cells. In contrast, both Raf-1 and B-Raf played an important role in inducing the sharp increase in ERK phosphorylation that occurs at the onset of PC differentiation.

Results

B cell–specific combined inactivation of *Braf* and *Raf1* decreases B cell numbers in the periphery

To analyze the role of Raf-1 and B-Raf in B cell development and activation, homozygous floxed *Raf1* (*Raf1*$^{fl/fl}$), *Braf* (*Braf*$^{fl/fl}$) or double floxed mice (*Braf*$^{fl/fl}$//*Raf1*$^{fl/fl}$) were mated to the Mb1-Cre strain (*12*) to generate *Raf1*$^{fl/fl}$//*Mb1-Cre* (Raf-1 KO), *Braf*$^{fl/fl}$//*Mb1-Cre* (B-Raf KO) and *Braf*$^{fl/fl}$//*Raf1*$^{fl/fl}$//*Mb1-Cre* (DKO) mice. The combination of the conditional *Raf* alleles with the Mb1-Cre strain resulted in B cell–specific deletion of the floxed *Raf* exons (fig. S1, A and B) and the absence of B-Raf and Raf-1 proteins in B cells (fig. S1C) after Cre-mediated recombination (fig. S1C).

Raf-1 KO and DKO mice displayed reduced total B cell numbers in the BM (Fig. 1A). To define whether the B cell reduction was due to a block in B cell development, we examined the different B cell populations in the BM using fluorescence-activated cell

sorting (FACS) after staining for the surface markers CD43 and B220. B cells that develop from pro- to pre-B cells decrease their CD43 abundance. Some B cells migrate back from the periphery into the BM. In contrast to developing B cells, these so-called recirculating B cells, express higher amounts of B220 and are IgD^{+}. The FACS analysis revealed that the B cell reduction in the BM is mainly due to a reduction of pre- and immature ($CD43^{-}B220^{low}$) and recirculating ($CD43^{-}B220^{high}IgM^{+}IgD^{high}$) B cells (Fig. 1B and fig. S2, A to C). Higher percentages of $CD43^{+}B220^{low}$ B cells in DKO mice in comparison to controls suggested a partial maturation block from pro- to pre-B cells (fig. S2A). To further delineate this differentiation block, $CD43^{+}B220^{low}$ (pro- and early pre-B cells) cells were further subdivided in Hardy´s fractions A to C´ by FACS after staining for the surface markers BP-1 and CD24 (*2*) (Fig. 1C). The presence of these two markers increases when pro-B cells proceed in their development from fraction A to C´. In DKO B cells, the percentage of fraction C was increased whereas that of fraction C´ was decreased (fig. S2D), resulting in a significantly lower ratio between the percentages from fraction C´ ($CD24^{high}BP\text{-}1^{+}$) and fraction C ($CD24^{+}BP\text{-}1^{+}$) in DKO mice than in the other genotypes (Fig. 1D). These data indicated an impaired transition from late pro- to early pre-B cells in B cells lacking functional *Braf* and *Raf1* genes.

Splenic weights and B cell numbers were significantly decreased in DKO mice in comparison to the control (Fig. 2A). The B cell reduction affected mostly Fo B ($CD21^{+}CD23^{high}$) cells, which were, in contrast to MZB ($CD21^{high}CD23^{low}$) cells, significantly reduced (Fig. 2, B and C). The splenic architecture, including a clear separation between B- and T-cell zones and the marginal zone, was preserved in B-Raf KO and Raf-1 KO (SKO) and DKO mice (fig. S3A). In inguinal lymph nodes

(iLN), B cell numbers were comparable among the knockouts and controls (fig. S3B). In addition, the percentage of B1a cells ($B220^{low}CD5^{+}$) was lower in the peritoneal cavities of DKO mice in comparison to the control and SKO mice. Compared to the controls, RAF-1 KO mice showed a slight decrease in the percentages of B1a cells. (Fig. 2D, fig. S3C). Taken together, these data suggested a function for B-Raf and Raf-1 in controlling the development and/or maintenance of Fo B and B1a cells.

Deficiency of B-Raf and Raf-1 impairs the influx and differentiation of immature B cells in the periphery

To investigate whether the reduced Fo B cell numbers in the spleens of DKO mice were caused by impaired influx or differentiation of immature B cells, we analyzed the amount of transitional $AA4.1^{+}IgM^{high}CD23^{-}$ (T1), $AA4.1^{+}IgM^{high}CD23^{+}$ (T2), and $AA4.1^{+}IgM^{low}CD23^{+}$ (T3) B cells in the spleens of all three knockout genotypes and controls by FACS. The numbers of transitional B cell subsets were decreased in the spleens of DKO and SKO mice in comparison to controls, indicating a reduced influx or differentiation in the absence of RAFs (Fig. 3A). The T2 population was more affected than the T1 population, resulting in a decreased T2/T1 ratio in mutant compared to control mice (Fig. 3B). These data illustrate a partial maturation block from T1 to T2. A less pronounced phenotype was detected in SKO mice (Fig. 3B), suggesting that B-Raf and Raf-1 act together in supporting the survival and differentiation of transitional B cells.

To determine the influx of immature B cells from the BM into the periphery and to investigate the survival of mature B cells, we performed Bromodeoxyouridine (BrdU) pulse-chase experiments (Fig. 3C). Because proliferation of B cells takes place

mainly during their development in the BM, mostly recent emigrants from the BM are labelled with BrdU at the end of the pulse. The percentages of $BrdU^+$ B cells at the end of the pulse were significantly lower in Raf-1 KO and DKO mice than in B-Raf KOs or controls (Fig. 3C), indicating a reduced efflux of newly formed B cells from the BM into the periphery. This phenotype is in accord with the decreased numbers of immature B cells ($CD43^-B220^{low}$) in the BM of RAF-1 KO and DKO mice (Fig. 1B). Setting $BrdU^+$ cells at the end of the pulse (day 14) to 100% yielded nearly the same decline in the percentages of $BrdU^+$ B cells in all four genotypes at days 42 and 70 after the pulse (Fig. 3C), indicating a comparable life span of mature B cells in the periphery. Thus, in comparison to controls, Raf-1 KO and DKO mice had a reduced B cell efflux from the BM, but the survival and persistence of mature B cells in the periphery was comparable among all four genotypes. Consistent with these findings, splenic B cells isolated from mice of all four genotypes showed similar survival when cultured in vitro in the presence or absence of CD40 stimulation (Fig. 3D). Collectively, these data demonstrate that the reduced B cell numbers in the spleens of DKO mice were caused by impaired influx and differentiation of newly generated B cells.

B-RAF and RAF-1 DKO mice have impaired immune responses

We analyzed the humoral immune responses in mice lacking B-Raf and/or Raf-1. To study the TD immune response, mice were immunized with the TD antigen nitrophenyl chicken-γ-globulin (NP-CGG) and analyzed 14 days later. Immunohistochemical analysis of the spleens showed GCs with a comparable structure and size (Fig. 4A), and FACS analysis revealed comparable percentages of GC (PNA^+CD95^+) B cells (Fig. 4B, fig. S4A) in control and mutant mice. However,

NP-specific IgM and IgG1 antibody titers were lower in DKO mice than in controls or SKO mice (Fig. 4C), suggesting impairment of TD immune responses in the absence of B-Raf and Raf-1.

To analyze whether TI immune responses were comparably affected, we immunized DKO and control mice with NP-LPS (a TI-1 antigen) and NP-Ficoll (a TI-2 antigen). Seven days after immunization with NP-LPS, the percentages of total plasmablasts (Fig. 4D), the amounts of NP-specific IgM, IgG1, IgG3, and IgA antibody-secreting cells (ASCs) (Fig. 4E and fig. S4B), as well as the NP-specific IgM, IgG1, IgG2a, and IgG3 antibody titers in the serum (Fig. 4F) were decreased in DKO mice in comparison to controls. Similarly, immunization with NP-Ficoll resulted in reduced numbers of NP-specific IgM and IgG3 ASCs in the spleen and decreased titers of NP-specific antibody titers in the serum in DKO mice in comparison to controls (fig. S4, C and D). Altogether, our data suggest that plasma cell (PC) differentiation was impaired upon immunization of DKO mice.

LPS-stimulated DKO B cells are impaired in proliferation and PC differentiation

To test whether the reduced antibody production in DKO mice upon immunization was due to the reduced number of B cells or to impaired PC differentiation, we compared the ability of B cells from DKO and control mice to differentiate into plasmablasts (PBs) in vitro. To this aim, splenic B cells were isolated and cultured with lipopolysaccharide (LPS) for 3 days and subsequently stained for markers that are either increased or decreased during the course of PC differentiation (Fig. 5A). We found that on day 3 of LPS stimulation the percentage of PB ($CD138^{high}B220^{low}$) cells in the cultures was sharply reduced in cells from DKO mice relative to cells from

control mice (Fig. 5B, fig. S5A). In DKO B cells, LPS stimulation increased IRF4 production (fig. S5B), but the percentage of BLIMP-1^{+} B cells was strongly reduced compared to control B cells (Fig. 5C). Moreover, the remaining BLIMP-1^{+} DKO B cells failed to adopt a PB phenotype (B220^{low}CD138^{+}) (Fig. 5D). Furthermore, the percentages of the Irf4^{high}Pax5^{low} cell population containing the pre-PBs and PBs were significantly reduced in DKO B cells (Fig. 5E). Within the fraction of IRF4^{high}PAX5^{low} cells, PB (B220^{low}CD138^{high}) cells were more strongly reduced than were pre-PB (B220^{+}CD138^{med}) cells (Fig. 5F, fig. S5C). These data imply that DKO B cells could still be properly activated but were strongly impaired in their transition from activated B cells to pre-PB cells as well as in their further differentiation into PBs.

Because B cells must divide several times before they differentiate into quiescent PCs, we asked whether impaired proliferation is responsible for the block in PC differentiation of DKO B cells. DKO B cells proliferated to a lesser extent than did control B cells upon LPS stimulation (Fig. 5G). In addition, the percentage of CD138^{high}B220^{low} PB cells in each cell division was reduced in DKO cells in comparison to control B cells (Fig. 5H, fig. S5D), indicating that the reduced PC percentages were not only due to decreased proliferation of DKO B cells but also to a defect in PC differentiation.

MEK and ERK are phosphorylated in the absence of B-Raf and Raf-1

Activation of Erk1 and Erk2 (ERK1/2) is essential for the differentiation of B cells to PCs (*11*). Because B-Raf and Raf-1 are part of the RAF-MEK-ERK signaling cascade, we hypothesized that PC differentiation of B cells from DKO mice was impaired due to reduced ERK phosphorylation. However, phosphorylated ERK

(pERK) amounts increased in DKO B cells during LPS stimulation and were even slightly higher than in control B cells at day 3 (Fig. 6A). Additionally, short-term stimulation with LPS and an antibody specific for IgM induced ERK1/2 phosphorylation in both DKO and control cells, reaching higher amounts of pERK in DKO than in control B cells (Fig. 6, B and C, fig. S6, A and B). Amounts of phosphorylated MEK (pMEK) followed a similar trend as pERK, being slightly higher in DKO than in control B cells (Fig. 6, B and C, fig. S6, A and B). Furthermore, DKO B cells exhibited increased and prolonged amounts of pERK in the nucleus upon LPS stimulation (Fig. 6D). FACS analysis confirmed that inactivation of B-Raf and Raf-1 led to significantly increased basal amounts of pERK in splenic Fo B and MZ B cells (Fig. 6E), as well as in recirculating B cells of the BM (Fig. 6, F and G). In contrast, in all other analyzed B cell populations of the BM, ERK phosphorylation was comparable in DKO and control mice and was lower than in recirculating B cells (Fig. 6G). These data suggest that in mature B cells, ERK phosphorylation is independent of B-Raf and Raf-1. Furthermore, RAFs are most likely involved in a negative feedback loop attenuating ERK phosphorylation in mature B cells.

Chemical RAF-inhibitors increase the ERK-phosphorylation in mature B cells

A-Raf, the third member of the RAF family, was comparably abundant in B cells from control and DKO mice (fig. S7A). To determine whether A-Raf mediated the phosphorylation of ERK in DKO B cells, we measured ERK phosphorylation in B cells from DKO mice in the presence of the pan-RAF inhibitors Sorafenib, Dabrafenib, and LY3009120. We included LY3009120 in our analysis because it induces no or only minimal paradoxical ERK activation and inactivates all three RAF isoforms with equivalent efficiency (*13*). All three pan-RAF inhibitors resulted in an

increase in ERK phosphorylation in control B cells that were unstimulated or treated with an IgM-specific antibody (Fig. 7, A and B, fig. S7, B to E). Moreover, neither LY3009120 nor Sorafenib attenuated ERK phosphorylation in DKO B cells that were unstimulated or IgM-stimulated (Fig. 7, A and B, fig. S7E). Similarly, LY3009120 did not reduce ERK phosphorylation in LPS-treated B cells and instead resulted in increased amounts of pERK (fig. S7F). These data indicate that A-RAF does not mediate the ERK phosphorylation in the absence of B-Raf and Raf-1. Moreover, these results show that both pharmacological RAF inhibition and genetic inactivation of B-Raf and Raf-1 increased the amounts of pERK in mature B cells.

In B cells, ERK is phosphorylated by the PI3K-AKT and RAC-PAK pathways

We next analyzed whether the absence of B-Raf and Raf-1 had any effect on other BCR-induced signaling pathways. BCR stimulation induces rapid phosphorylation of its immunoreceptor tyrosine-based activation motifs (ITAMs) followed by the recruitment of the tyrosine kinase SYK. Phosphorylated SYK activates several downstream pathways, such as phospholipase-Cγ2 (PLC-γ2), nuclear factor κB (NF-κB), and PI3K-Akt signaling as well as the MAP kinases c-Jun N-terminal kinases (JNKs), ERK, and p38. We did not detect any significant differences in the activation of SYK or its downstream targets in DKO cells compared to control B cells upon IgM stimulation (fig. S8, A to E). To better understand which signaling pathways led to the activation of ERK in the absence of B-Raf and Raf-1, we investigated BCR-induced ERK phosphorylation in the presence of chemical inhibitors. Inhibition of SYK phosphorylation by the addition of p505-15 strongly reduced ERK phosphorylation in stimulated and unstimulated B cells (Fig. 7C, fig. S9A), suggesting that activation of SYK is essential for ERK phosphorylation. To further

dissect the signaling pathways resulting in ERK phosphorylation downstream of SYK, we treated the B cells with chemical inhibitors targeting the PI3K-AKT, RAC-PAK (p21-activated kinase), and NF-κB signaling pathways (*14*). Both the AKT inhibitor AKTi-1/2 (Fig. 7C, fig. S9A) and the PI3K inhibitor LY294002 (Fig. 7D, fig. S9B) partially attenuated ERK phosphorylation in B cells stimulated with an IgM-specific antibody. The SYK, AKT, and PI3K inhibitors also abolished AKT phosphorylation as expected, demonstrating the successful inhibition of the respective signaling molecules (Fig. 7, C and D, fig. S9, A and B). These data indicate that in DKO B cells, ERK was activated at least partially by PI3K-AKT signaling. Earlier data suggested that PAK, which can activated by RAC either PI3K-dependently or -independently, activates ERK (*15-18*). Indeed, addition of the PAK inhibitor PF-3758309 also diminished ERK phosphorylation (Fig. 7E, fig. S9C), whereas the NF-κB inhibitor IKK2-inhibitor8 did not influence pERK amounts (fig. S9D). PI3K-dependent ERK phosphorylation seemed also to occur upon LPS stimulation, because inhibition of PI3K signaling by LY294002 decreased pERK amounts in LPS-stimulated B cells (fig. S9E). These data suggest that in B cells, ERK is activated by Raf-independent signaling pathways, such as PI3K-AKT and RAC-PAK, whereas the RAFs appear to affect the amounts of pERK negatively.

To test whether ERK phosphorylation was essential for the survival of B cells, we treated LPS-stimulated splenic B cells from control and DKO mice with the MEK inhibitor UO126 and analyzed the survival of LPS-stimulated B cells after three days of culture. UO126 strongly impaired the ex vivo survival of isolated B cells from both genotypes (fig. S10A). The few remaining control and DKO B cells that survived culture in the presence of UO126 had amounts of pERK similar to those in DMSO-

treated control cells (fig. S10B). These data imply that a certain amount of ERK activation is necessary for the survival of B cells in vitro.

ERK phosphorylation is reduced in pre-PBs of DKO mice

Our data suggested that the impaired PC differentiation of B cells from DKO mice was not due to a reduction in ERK phosphorylation during initial B cell activation. Because genetic inactivation of ERK1/2 showed a very similar phenotype in PC differentiation (*11*) as did the inactivation of Raf-1 and B-Raf, we wondered whether ERK phosphorylation in DKO B cells was disturbed during PC differentiation. To address this question, we quantified pERK and total ERK in ex vivo isolated unstimulated B cells (naïve B cells ($IRF4^{low}PAX5^{high}$) d0), and in B cells that were stimulated with LPS for 3 days. LPS stimulated B cells were be further subdivided in activated B cells ($IRF4^{int}PAX5^{high}$), pre-PBs ($IRF4^{high}PAX5^{low}CD138^{low}B220^{+}$), and PBs ($IRF4^{high}PAX5^{low}CD138^{high}B220^{low}$) (Fig. 8A and B). In B cells from control and DKO mice, the amounts of pERK increased similarly at the transition from naïve to activated B cells. However, at the transition from activated B cells to pre-PBs, controls showed a very strong increase in pERK amounts, whereas this increase was significantly diminished in DKO B cells (Fig. 8, C and D). Total amounts of ERK increased slightly and comparably in both control and DKO B cells over the course of PC differentiation (Fig. 8, C and D). Calculation of the pERK/ERK ratio at different stages of B cell differentiation revealed that significantly more ERK was phosphorylated in pre-PBs and PBs from control mice compared to cells from DKO mice (Fig. 8E). To exclude that the remaining PBs generated from DKO B cells originated from B cells that had not deleted the floxed *Braf* and *Raf-1* exons, we amplified the loxP-flanked DNA region in DKO and control mice from B cells that

were cultured in the presence of LPS. At day 3, $CD19^{+}CD138^{-}B220^{+}$ B2 cells and $CD19^{+}CD138^{high}B220^{low}$ PBs were sorted (fig. S11A). In both B cell populations from DKO mice, we detected only the deleted but not the floxed alleles (fig. S11B). These results confirm that the few PBs that were generated in DKO mice did not have intact *Braf* or *Raf1* alleles.

We conclude from these data that B-Raf and Raf-1 are neither essential for basal ERK phosphorylation in naïve B cells nor for the increased ERK phosphorylation in activated B cells. However, RAFs are needed to mediate the strong enhancement of ERK phosphorylation at the transition from activated B cells to pre-PBs. Notably, in DKO mice, the partial block in PC differentiation coincided with the differentiation stage in which ERK phosphorylation strongly increases. These data suggest that a sharp increase in ERK phosphorylation is a prerequisite for PC differentiation. We suppose that only a small number of DKO B cells reach this threshold amount of pERK, explaining the strong drop in the percentages of pre-PB and PB in DKO in comparison to control mice.

Discussion

Throughout their development and activation, B cells depend on signals from the BCR and members of the TNF-R family, such as CD40 and the B-cell activating factor receptor (BAFF-R), all of which activate the MAPK-ERK pathway (*4, 19-24*). Although it is well established that the kinases RAF take part in MAPK signaling upstream of MEK1/2, the specific role of the three different RAF family members in B cell development and activation is still elusive. We describe here a function of B-Raf

and Raf-1 in the transition of pro-B cells to pre-B cells, in the differentiation of transitional B cells to mature B cells, and in the differentiation of PCs.

Several lines of evidence suggest that the RAS-RAF-MEK-ERK signaling pathway is activated downstream of the pre-BCR and is involved in the positive selection of pre-B cells (*5-7, 25-27*). However, the role of RAFs in this selection process has not been analyzed in detail. Our data imply that B-Raf and Raf-1 act together in mediating positive selection downstream of the pre-BCR, with Raf-1 apparently playing a more prominent role than B-Raf. We did not detect any difference in pERK amounts in pro- and pre-B cells between DKO and control mice, perhaps because only B cells that reach a certain amount of ERK phosphorylation can survive the selection processes in pre-B cells and transitional B cells.

Impaired survival and/or differentiation of pre-B cells in the BM and T2 cells in the spleen resulted in strongly reduced B cell numbers in the periphery of DKO mice compared to control mice. Mature B cells from DKO mice could still form GCs but were impaired in their PC differentiation in vivo and in vitro. Because ERK1/2 DKO B cells show a similar defect in PC differentiation (*11*) we expected the block of PC differentiation in DKO mice to be due to impaired ERK phosphorylation upon stimulation. However, unexpectedly, ERK phosphorylation was not attenuated in naïve or activated DKO B cells and was even higher than in DKO B cells than in control B cells. Only at the onset of PC differentiation, when, as we have shown here, ERK phosphorylation sharply increases, was ERK phosphorylation reduced by the absence of B-Raf and Raf-1.

Comparably to the genetic inactivation of B-Raf and Raf-1, ERK phosphorylation also increased after addition of chemical pan-RAF inhibitors. The increase in ERK phosphorylation in the presence of pan-RAF inhibitors must be interpreted with caution, because low concentrations of pan-RAF inhibitors, such as Dabrafenib and Sorafenib, can lead to paradoxical MEK-ERK activation by inducing RAF dimerization (*28-31*). However, the several points suggest that the increased ERK phosphorylation was not caused by paradoxical ERK activation in our experiments. First, ERK phosphorylation increased in B cells with increasing amounts of RAF-inhibitors, whereas paradoxical ERK activation is mainly observed by the addition of low concentrations of RAF inhibitor (*28, 31*). Secondly, the pan-RAF inhibitor LY3009120, which has been described to induce no or only minimal paradoxical ERK activation (*13*), increased ERK phosphorylation comparably to Sorafenib and Dabrafenib. Moreover, ERK phosphorylation was increased by both genetic inactivation and by chemical inhibition of B-Raf and Raf-1. Thus, our data suggest that in mature murine B cells, kinases of the RAF family are not essential for ERK phosphorylation, but are rather involved in a negative feedback loop.

Murine B cells also produce the third family member, A-Raf, which might form homodimers in the absence of B-Raf and Raf-1 and thus activate the MEK-ERK signaling pathway (*32*). However, because even the paradox-breaking inhibitor LY3009120, which inhibits A-Raf, B-Raf, and Raf-1 with similar efficiencies (*13*), did not attenuate ERK phosphorylation in control or DKO B cells, we assume that A-Raf is not the main player for ERK activation in B cells. Instead, our data indicate that ERK activation is mediated by various RAF-independent signaling pathways acting downstream of SYK, such as PI3K-AKT and RAC-PAK. PAK, a serine-threonine

kinase, is activated through RAC either PI3K-dependently or PI3K-independently (*16-18, 33*). Both PI3K and PAK as well as PLC-γ have been described earlier to promote the activation of ERK (*14, 17, 33-36*). These data suggest that ERK is activated in naïve and activated B cells through a concerted action of PI3K-AKT, RAC-PAK, and PLC-γ, whereas RAFs appear to attenuate ERK phosphorylation in naïve and activated B cells even though they are the main signaling molecules that usually induce the phosphorylation of MEK-ERK in other contexts (Fig. 8F).

This RAF-dependent negative feedback loop may be mediated by dual-specificity MAP kinase phosphatases (MKPs/DUSPs), such as DUSP5 and DUSP6, which dephosphorylate and inactivate ERK (*37*). It has been suggested that RAFs are involved in modulating the function and production of DUSP5 (*38*). Thus, deregulation of DUSP5 in RAF DKO B cells might lead to the disturbed ERK phosphorylation we observed in naïve and activated B cells. The negative effect of RAF kinases on pERK amounts may be a peculiarity of B cells, in which tonic BCR signaling is constitutively active. Thus, a negative regulatory mechanism might be required to prevent overshooting of ERK phosphorylation to protect naïve and activated B cells from premature differentiation into PCs.

A negative regulatory function of RAFs appears to have arisen later in evolution, because inactivation of B-Raf and Raf-1 in the chicken lymphoma DT40 cell line prevents phosphorylation of ERK after stimulation with an IgM-specific antibody (*39*). In contrast, kinases of the RAF family seem to act as positive regulators during the course of PC differentiation, mediating the steep rise in ERK phosphorylation that is a prerequisite for the initiation of PC differentiation (Fig. 8F). Constitutively increased

ERK phosphorylation in DKO B cells may further contribute to the attenuated increase in ERK phosphorylation at the onset of PC differentiation. Earlier results underline this hypothesis: Continuous BCR stimulation resulting in continuous ERK phosphorylation inhibits PC differentiation triggered by Toll-like receptors (TLRs). Moreover, anergic B cells, which are continuously triggered by self-antigen and therefore have constantly high ERK phosphorylation, are strongly impaired in PC differentiation (*40-42*). It has been noted that, on the one hand, ERK phosphorylation is coupled with cell division in B lymphocytes but, on the other hand, is necessary to induce PC differentiation that is coupled with cell cycle arrest (*43*). We now provide evidence that different amounts of ERK activation influence the cell fate of activated B cells. Thus, moderate amounts of ERK phosphorylation may be coupled with proliferation, whereas a high intensity of ERK activation induces PC differentiation. Maximal ERK phosphorylation is also essential for other differentiation processes such as the development of the central nervous system, in the skin, and during embryogenesis (*44*).

Collectively, we present here the finding that kinases of the RAF family dampen rather than stimulate ERK phosphorylation in naïve and activated B cells. Furthermore, we provide evidence for an important function of RAF kinases in the regulation of ERK phosphorylation during PC differentiation. Our data may have some implications for the clinic. Our results demonstrating the important function of RAFs during PC differentiation suggest that constitutive active RAF signaling may enhance PC differentiation and may explain why 4% of multiple myelomas harbor the activating $BRAF^{V600E}$ mutation (*45*). Taking into account the negative regulatory function of RAF kinases on ERK phosphorylation in B cells, one might predict that

treatment of most B cell lymphomas with pan-RAF inhibitors would increase rather than decrease ERK phosphorylation.

Materials and Methods

Antibodies

The different antibodies used in FACS, ELISA, ELISpot, Western blot, protein simple WES (WES) and Immunohistochemistry (Histo), their conjugation, the clone name and the company as well as their dilutions are listed in table S1.

Mice

Raf1$^{fl/fl}$ (*46*), *Braf*$^{fl/fl}$ (*47*), and *Raf1*$^{fl/fl}$/*Braf*$^{fl/fl}$ mice were crossbred to Mb1-cre mice (*12*) resulting in deletion of the *Raf* genes from early B cell development onwards. All mouse strains were on a C57BL/6 background and were analyzed at 8-20 weeks of age. The B cell phenotype in the BM and secondary lymphoid organs was examined in the single transgenic (SKO) and double transgenic (DKO) mice. For further analysis of the PC differentiation, we concentrated on the DKO mice. As controls Mb1-Cre or WT mice were used, which had in our analyses the same phenotype. Analyses were performed on both male and female mice and data were analyzed in an unblinded way. Control and mutant mice were always examined in parallel. Primers for the amplification of the floxed RAF-genes are listed in table S2. Sample sizes, numbers of independent experiments and statistical analyses are described in the figure legends.

Mice were maintained in specific pathogen-free conditions. Experiments were performed in accordance to the German Animal Welfare Act and were approved by

the institutional committee on animal experimentation and the Government of Upper-Bavaria.

Mouse immunizations

For immunization 8- to 16-weeks-old mice were injected intraperitoneally with either 100µg alum-precipitated nitrophenylacetyl chicken gamma globulin (NP-CGG; Biosearch Technologies, Novato, CA), 50µg NP-Ficoll (Biosearch Technologies) or 25 µg NP-LPS (LGC Biosearch). Mice were analyzed 14 days after immunization with NP-Ficoll or 7 days after immunization with NP-LPS.

Cell purification and in vitro cultures

B cells were isolated from splenic cell suspensions by depleting $CD43^+$ cells with magnetic beads (Miltenyi Biotec). As indicated in each figure, splenic B cells were cultivated up to five days to test their survival in vitro and up to 3 days to analyze their proliferation and PC differention upon LPS stimulation in vitro. Therefore, splenic B cells were cultivated in RPMI medium supplemented with 10 % (v/v) heat-inactivated fetal calf serum (FCS) (PAA Cell culture Company), 1 % (v/v) penicillin/streptomycin, 1 % (v/v) sodium pyruvate, 1 % (v/v) L-glutamine, and 50µM β-mercaptoethanol. Except for FCS, all supplements were purchased from Gibco. As stimuli lipopolysaccharide (10 µg/ml; E.coli 055:B5; Sigma) or an agonistic antibody against CD40 (2.5 µg/ml; eBioscience [HM40-3]) were used. For proliferation assays, B cells were stained with 5µM 5-(and 6)-carboxyfluorescein diacetate N-succinimidyl ester (CFSE) (Molecular Probes) for five minutes at 37°C before culturing them. To analyze the signaling pathways after short time stimulation, B cells were stimulated either with an antibody specific for IgM (15µg/ml; AffiniPure F(ab')2 goat anti-mouse

IgM, µ-chain, Dianova) for 2.5min or with lipopolysaccharide (10 µg/ml; E.coli 055:B5; Sigma) for 1min or 5min. The stimulation was performed in RPMI containing 1% FCS plus supplements. Prior to stimulation, the B cells were incubated in RPMI with 1% FCS and supplements for 1 hour. B cells were incubated with small chemical inhibitors against the RAF-kinases in different concentrations as indicated in the figures. The following inhibitors were used in our assays: (i) RAF-inhibitors: LY3009120 (0.1µM-10µM), Selleckchem; Sorafenib (1µM-10µM), Bayer HealthCare; Dabrafenib (1µM-10µM), Selleckchem; (ii) PI3-kinases inhibitor: LY294002 (6µM or 20µM), Cell Signaling Technology; (iii) SYK-kinase inhibitor: P505-15 (0.5µM), Selleckchem; (iv) PAK-kinase inhibitor: PF-3758309 (5µM or 10µM), Sellekchem; (v) AKT-kinase inhibitor: AKT8=AKTi-1/2 (5µM), Merck; (vi) IKK2 inhibitor: IKK2-inhibitor8 (5µM), Merck; (vii) MEK-kinase inhibitor: UO126 (10µM), Cell Signaling Technology, Inc. The solvent of the inhibitor DMSO (Dimethylsulfoxide, Sigma Life Science) was used as control. Inhibitor treatment of the cells: Before stimulation, B cells were incubated in RPMI containing 1% FCS plus supplements for half an hour in the absence of the inhibitor and then for 1.5 hours in the presence of the inhibitor.

ELISA and ELISpot

ELISA was performed as described in Rastelli *et al*. (*48*). The absorbance was measured in an ELISA reader (Photometer Sunrise RC, Tecan) at OD_{405}. For antigen-specific ELISpot, 96-well plates for ELISpots (Milipore) were coated with NP_4- or NP_{16}-BSA (Biosearch Technologies). ELISpot analyzes were performed as described (*48, 49*). Spots were analyzed and counted with the ImmunoSpot Series 5 UV Analyzer (CTL-Europe). The antibodies used are listed in Table S1.

FACS

Antibodies used for flow cytometry are listed in Table S1. The primary antibody against ERK, phospho-ERK (pT202/pY204) and their isotype control (DA1E) were stained by the goat anti-rabbit IgG (H+L) (Invitrogen). For intracellular FACS stainings (BLIMP1, PAX5, IRF4, ERK, and phospho-ERK), cells were fixed with 2% paraformaldehyde and permeabilized with methanol. To include only living cells into the analysis, cells were stained for 5min on ice either with TO-PRO-3 (Molecular Probes) prior to the FACS analysis or with LIVE/DEAD™ Fixable Blue Dead Cell Stain Kit (invitrogen) prior to fixation of the cells. FACS data were acquired with a FACSCalibur™ or FACSFortessa (BD Biosciences). Results were evaluated using CellQuest™ or FlowJo (Treestar).

BrdU pulse-chase experiment

Pulse-chase BrdU experiments were performed to determine the survival of B cells in vivo. Mice were fed with 0.8 mg/ml BrdU in their drinking water for 14 days during the pulse period. The $BrdU^+$ cells in the blood were tracked until day 70 during the chase period. Blood samples were taken at days 7, 14, 42 and 70. Percentages of $BrdU^+$ B cells were determined by flow cytometry analysis using the APC BrdU Flow Kit (BD Bioscience).

Immunohistochemistry

Histology was performed as described in (*50*). The antibodies used are listed in Table S1. Slides were evaluated with an Axiovert 135 (Zeiss, Jena, Germany) microscope with PL 10x/20 eyepiece and a 10x/0.30 Plan-Neofluar objective lens. Pictures obtained with a RS Photometrics digital camera (Tucson, AZ) were processed with Adobe Photoshop CS3 software.

Western blot analysis

Protein extract preparation and Western blot analysis were performed as previously described by Hömig-Hölzel *et al*. (*21*). The antibodies used for Western blot analysis are listed in Table S1. The Western blots were analyzed either by film (Agfa Healthcare) exposition, subsequent development and scanning (EPSON Expression-1680Pro Scanner) or by the Vilber Fusion FX6 Edge imager. For quantification of the analogous films ImageJ/Fiji was used. The digital images were quantified by the Vilber Bio-1D software. The abundance of the different proteins were normalized to their inherent loading control (Tubulin or GAPDH). The fold increase in protein amounts was calculated by dividing the normalized abundance of the protein in each sample by the normalized abundance of the protein in the inherent control samples.

ProteinSimple WES

B cells were kept unstimulated or were stimulated with lipopolysaccharide (10 µg/ml; E.coli 055:B5; Sigma) between 0.5min and 20min in RPMI containing 1% FCS plus supplements. Nuclear extracts were isolated using the NE-PERKit (ThermoScientific, Waltham, MA). The pERK and Lamin B2 (antibodies see Table S1) protein abundances were analyzed by the WES system (ProteinSimple), according to the manufacturer's instructions.

Statistics

The Prism software (version 7-9, GraphPad software) was used to perform all the statistical analyses including testing for distributions and equal variances, calculating means, standard deviations and performing ANOVA. This software was also used to

obtain all the statistical plots. The different tests for statistical analyzes are indicated in the Figure legends. Experiments and analysis were not performed in a blinded manner.

Supplementary Materials:

Fig. S1. Deletion of *Braf* and *Raf1* in B cells from SKO and DKO mice

Fig. S2. B cell subpopulations in the BM

Fig. S3. Mature B cells in the periphery

Fig. S4. TD and TI immune responses in RAF-deficient mice

Fig. S5. Plasma cell differentiation upon LPS stimulation in vitro

Fig. S6. Abundance of pMEK and pERK in unstimulated and stimulated B cells

Fig. S7. ERK phosphorylation in the presence of pan-RAF inhibitors

Fig. S8. Activation of signaling pathways downstream of the BCR

Fig. S9. RAF-independent ERK phosphorylation in mature B cells

Fig. S10. Survival of B cells in the presence of the MEK inhibitor UO126

Fig. S11. Deletion of the floxed exons in PCs

Table S1. Antibodies used in this study

Table S2. Primers for PCR amplification of the *Raf* genes

References and Notes

1. D. Matallanas, M. Birtwistle, D. Romano, A. Zebisch, J. Rauch, A. von Kriegsheim, W. Kolch, Raf family kinases: old dogs have learned new tricks. *Genes Cancer* **2**, 232-260 (2011).
2. R. R. Hardy, K. Hayakawa, B cell development pathways. *Annu Rev Immunol* **19**, 595-621 (2001).
3. M. D. Thomas, B. Srivastava, D. Allman, Regulation of peripheral B cell maturation. *Cell Immunol* **239**, 92-102 (2006).
4. S. L. Rowland, C. L. DePersis, R. M. Torres, R. Pelanda, Ras activation of Erk restores impaired tonic BCR signaling and rescues immature B cell differentiation. *J Exp Med* **207**, 607-621 (2010).

5. B. M. Iritani, K. A. Forbush, M. A. Farrar, R. M. Perlmutter, Control of B cell development by Ras-mediated activation of Raf. *EMBO J* **16**, 7019-7031 (1997).
6. A. C. Shaw, W. Swat, R. Ferrini, L. Davidson, F. W. Alt, Activated Ras signals developmental progression of recombinase-activating gene (RAG)-deficient pro-B lymphocytes. *J Exp Med* **189**, 123-129 (1999).
7. T. Yasuda, H. Sanjo, G. Pages, Y. Kawano, H. Karasuyama, J. Pouyssegur, M. Ogata, T. Kurosaki, Erk kinases link pre-B cell receptor signaling to transcriptional events required for early B cell expansion. *Immunity* **28**, 499-508 (2008).
8. Y. Chen, Y. Zheng, X. You, M. Yu, G. Fu, X. Su, F. Zhou, W. Zhu, Z. Wu, J. Zhang, R. Wen, D. Wang, Kras Is Critical for B Cell Lymphopoiesis. *J Immunol* **196**, 1678-1685 (2016).
9. L. S. Teodorovic, C. Babolin, S. L. Rowland, S. A. Greaves, D. P. Baldwin, R. M. Torres, R. Pelanda, Activation of Ras overcomes B-cell tolerance to promote differentiation of autoreactive B cells and production of autoantibodies. *Proc Natl Acad Sci U S A* **111**, E2797-2806 (2014).
10. S. A. Greaves, J. N. Peterson, R. M. Torres, R. Pelanda, Activation of the MEK-ERK Pathway Is Necessary but Not Sufficient for Breaking Central B Cell Tolerance. *Front Immunol* **9**, 707 (2018).
11. T. Yasuda, K. Kometani, N. Takahashi, Y. Imai, Y. Aiba, T. Kurosaki, ERKs induce expression of the transcriptional repressor Blimp-1 and subsequent plasma cell differentiation. *Sci Signal* **4**, ra25 (2011).
12. E. Hobeika, S. Thiemann, B. Storch, H. Jumaa, P. J. Nielsen, R. Pelanda, M. Reth, Testing gene function early in the B cell lineage in mb1-cre mice. *Proc Natl Acad Sci U S A* **103**, 13789-13794 (2006).
13. S. B. Peng, J. R. Henry, M. D. Kaufman, W. P. Lu, B. D. Smith, S. Vogeti, T. J. Rutkoski, S. Wise, L. Chun, Y. Zhang, R. D. Van Horn, T. Yin, X. Zhang, V. Yadav, S. H. Chen, X. Gong, X. Ma, Y. Webster, S. Buchanan, I. Mochalkin, L. Huber, L. Kays, G. P. Donoho, J. Walgren, D. McCann, P. Patel, I. Conti, G. D. Plowman, J. J. Starling, D. L. Flynn, Inhibition of RAF Isoforms and Active Dimers by LY3009120 Leads to Anti-tumor Activities in RAS or BRAF Mutant Cancers. *Cancer Cell* **28**, 384-398 (2015).
14. C. Hojer, S. Frankenberger, L. J. Strobl, S. Feicht, K. Djermanovic, F. Jagdhuber, C. Homig-Holzel, U. Ferch, J. Ruland, K. Rajewsky, U. Zimber-Strobl, B-cell expansion and lymphomagenesis induced by chronic CD40 signaling is strictly dependent on CD19. *Cancer Res* **74**, 4318-4328 (2014).
15. P. R. Somanath, J. Vijai, J. V. Kichina, T. Byzova, E. S. Kandel, The role of PAK-1 in activation of MAP kinase cascade and oncogenic transformation by Akt. *Oncogene* **28**, 2365-2369 (2009).
16. Z. Wang, E. Pedersen, A. Basse, T. Lefever, K. Peyrollier, S. Kapoor, Q. Mei, R. Karlsson, A. Chrostek-Grashoff, C. Brakebusch, Rac1 is crucial for Ras-dependent skin tumor formation by controlling Pak1-Mek-Erk hyperactivation and hyperproliferation in vivo. *Oncogene* **29**, 3362-3373 (2010).
17. K. Jiang, B. Zhong, D. L. Gilvary, B. C. Corliss, E. Hong-Geller, S. Wei, J. Y. Djeu, Pivotal role of phosphoinositide-3 kinase in regulation of cytotoxicity in natural killer cells. *Nat Immunol* **1**, 419-425 (2000).
18. H. Ebi, C. Costa, A. C. Faber, M. Nishtala, H. Kotani, D. Juric, P. Della Pelle, Y. Song, S. Yano, M. Mino-Kenudson, C. H. Benes, J. A. Engelman, PI3K regulates MEK/ERK signaling in breast cancer via the Rac-GEF, P-Rex1. *Proc Natl Acad Sci U S A* **110**, 21124-21129 (2013).
19. S. L. Rowland, K. F. Leahy, R. Halverson, R. M. Torres, R. Pelanda, BAFF receptor signaling aids the differentiation of immature B cells into transitional B cells following tonic BCR signaling. *J Immunol* **185**, 4570-4581 (2010).
20. G. Metzler, N. S. Kolhatkar, D. J. Rawlings, BCR and co-receptor crosstalk facilitate the positive selection of self-reactive transitional B cells. *Curr Opin Immunol* **37**, 46-53 (2015).

21. C. Homig-Holzel, C. Hojer, J. Rastelli, S. Casola, L. J. Strobl, W. Muller, L. Quintanilla-Martinez, A. Gewies, J. Ruland, K. Rajewsky, U. Zimber-Strobl, Constitutive CD40 signaling in B cells selectively activates the noncanonical NF-kappaB pathway and promotes lymphomagenesis. *J Exp Med* **205**, 1317-1329 (2008).
22. K. L. Otipoby, Y. Sasaki, M. Schmidt-Supprian, A. Patke, R. Gareus, M. Pasparakis, A. Tarakhovsky, K. Rajewsky, BAFF activates Akt and Erk through BAFF-R in an IKK1-dependent manner in primary mouse B cells. *Proc Natl Acad Sci U S A* **105**, 12435-12438 (2008).
23. R. C. Rickert, New insights into pre-BCR and BCR signalling with relevance to B cell malignancies. *Nat Rev Immunol* **13**, 578-591 (2013).
24. E. Schweighoffer, L. Vanes, J. Nys, D. Cantrell, S. McCleary, N. Smithers, V. L. Tybulewicz, The BAFF receptor transduces survival signals by co-opting the B cell receptor signaling pathway. *Immunity* **38**, 475-488 (2013).
25. S. Herzog, M. Reth, H. Jumaa, Regulation of B-cell proliferation and differentiation by pre-B-cell receptor signalling. *Nat Rev Immunol* **9**, 195-205 (2009).
26. H. E. Fleming, C. J. Paige, Pre-B cell receptor signaling mediates selective response to IL-7 at the pro-B to pre-B cell transition via an ERK/MAP kinase-dependent pathway. *Immunity* **15**, 521-531 (2001).
27. B. M. Iritani, J. Alberola-Ila, K. A. Forbush, R. M. Perimutter, Distinct signals mediate maturation and allelic exclusion in lymphocyte progenitors. *Immunity* **10**, 713-722 (1999).
28. P. I. Poulikakos, C. Zhang, G. Bollag, K. M. Shokat, N. Rosen, RAF inhibitors transactivate RAF dimers and ERK signalling in cells with wild-type BRAF. *Nature* **464**, 427-430 (2010).
29. S. J. Heidorn, C. Milagre, S. Whittaker, A. Nourry, I. Niculescu-Duvas, N. Dhomen, J. Hussain, J. S. Reis-Filho, C. J. Springer, C. Pritchard, R. Marais, Kinase-dead BRAF and oncogenic RAS cooperate to drive tumor progression through CRAF. *Cell* **140**, 209-221 (2010).
30. G. Hatzivassiliou, K. Song, I. Yen, B. J. Brandhuber, D. J. Anderson, R. Alvarado, M. J. Ludlam, D. Stokoe, S. L. Gloor, G. Vigers, T. Morales, I. Aliagas, B. Liu, S. Sideris, K. P. Hoeflich, B. S. Jaiswal, S. Seshagiri, H. Koeppen, M. Belvin, L. S. Friedman, S. Malek, RAF inhibitors prime wild-type RAF to activate the MAPK pathway and enhance growth. *Nature* **464**, 431-435 (2010).
31. K. Miyamoto, M. Sawa, Development of Highly Sensitive Biosensors of RAF Dimerization in Cells. *Sci Rep* **9**, 636 (2019).
32. J. Mooz, T. K. Oberoi-Khanuja, G. S. Harms, W. Wang, B. S. Jaiswal, S. Seshagiri, R. Tikkanen, K. Rajalingam, Dimerization of the kinase ARAF promotes MAPK pathway activation and cell migration. *Sci Signal* **7**, ra73 (2014).
33. J. Y. Chu, I. Dransfield, A. G. Rossi, S. Vermeren, Non-canonical PI3K-Cdc42-Pak-Mek-Erk Signaling Promotes Immune-Complex-Induced Apoptosis in Human Neutrophils. *Cell Rep* **17**, 374-386 (2016).
34. W. G. King, M. D. Mattaliano, T. O. Chan, P. N. Tsichlis, J. S. Brugge, Phosphatidylinositol 3-kinase is required for integrin-stimulated AKT and Raf-1/mitogen-activated protein kinase pathway activation. *Mol Cell Biol* **17**, 4406-4418 (1997).
35. A. Hashimoto, H. Okada, A. Jiang, M. Kurosaki, S. Greenberg, E. A. Clark, T. Kurosaki, Involvement of guanosine triphosphatases and phospholipase C-gamma2 in extracellular signal-regulated kinase, c-Jun NH2-terminal kinase, and p38 mitogen-activated protein kinase activation by the B cell antigen receptor. *J Exp Med* **188**, 1287-1295 (1998).
36. A. Jacob, D. Cooney, M. Pradhan, K. M. Coggeshall, Convergence of signaling pathways on the activation of ERK in B cells. *J Biol Chem* **277**, 23420-23426 (2002).
37. A. M. Kidger, S. M. Keyse, The regulation of oncogenic Ras/ERK signalling by dual-specificity mitogen activated protein kinase phosphatases (MKPs). *Semin Cell Dev Biol* **50**, 125-132 (2016).
38. A. M. Kidger, L. K. Rushworth, J. Stellzig, J. Davidson, C. J. Bryant, C. Bayley, E. Caddye, T. Rogers, S. M. Keyse, C. J. Caunt, Dual-specificity phosphatase 5 controls the localized

inhibition, propagation, and transforming potential of ERK signaling. *Proc Natl Acad Sci U S A* **114**, E317-E326 (2017).
39. T. Brummer, P. E. Shaw, M. Reth, Y. Misawa, Inducible gene deletion reveals different roles for B-Raf and Raf-1 in B-cell antigen receptor signalling. *EMBO J* **21**, 5611-5622 (2002).
40. L. Rui, C. G. Vinuesa, J. Blasioli, C. C. Goodnow, Resistance to CpG DNA-induced autoimmunity through tolerogenic B cell antigen receptor ERK signaling. *Nat Immunol* **4**, 594-600 (2003).
41. L. Rui, J. I. Healy, J. Blasioli, C. C. Goodnow, ERK Signaling Is a Molecular Switch Integrating Opposing Inputs from B Cell Receptor and T Cell Cytokines to Control TLR4-Driven Plasma Cell Differentiation. *The Journal of Immunology* **177**, 5337-5346 (2006).
42. S. R. Lee, J. A. Rutan, A. J. Monteith, S. Z. Jones, S. A. Kang, K. N. Krum, M. A. Kilmon, J. R. Roques, N. J. Wagner, S. H. Clarke, B. J. Vilen, Receptor cross-talk spatially restricts p-ERK during TLR4 stimulation of autoreactive B cells. *J Immunol* **189**, 3859-3868 (2012).
43. D. M. Allman, M. P. Cancro, pERKing up the BLIMP in plasma cell differentiation. *Sci Signal* **4**, pe21 (2011).
44. C. Dorard, G. Vucak, M. Baccarini, Deciphering the RAS/ERK pathway in vivo. *Biochem Soc Trans* **45**, 27-36 (2017).
45. M. Chesi, P. L. Bergsagel, Molecular pathogenesis of multiple myeloma: basic and clinical updates. *Int J Hematol* **97**, 313-323 (2013).
46. V. Jesenberger, K. J. Procyk, J. Ruth, M. Schreiber, H. C. Theussl, E. F. Wagner, M. Baccarini, Protective role of Raf-1 in Salmonella-induced macrophage apoptosis. *J Exp Med* **193**, 353-364 (2001).
47. A. P. Chen, M. Ohno, K. P. Giese, R. Kühn, R. L. Chen, A. J. Silva, Forebrain-specific knockout of B-raf kinase leads to deficits in hippocampal long-term potentiation, learning, and memory. *Journal of Neuroscience Research* **83**, 28-38 (2006).
48. J. Rastelli, C. Homig-Holzel, J. Seagal, W. Muller, A. C. Hermann, K. Rajewsky, U. Zimber-Strobl, LMP1 signaling can replace CD40 signaling in B cells in vivo and has unique features of inducing class-switch recombination to IgG1. *Blood* **111**, 1448-1455 (2008).
49. S. A. Sperling, P. Fiedler, M. Lechner, A. Pollithy, S. Ehrenberg, A. I. Schiefer, L. Kenner, A. Feuchtinger, R. Kuhn, G. Swinerd, M. Schmidt-Supprian, L. J. Strobl, U. Zimber-Strobl, Chronic CD30-signaling in B cells results in lymphomagenesis by driving the expansion of plasmablasts and B1 cells. *Blood*, (2019).
50. F. Hampel, S. Ehrenberg, C. Hojer, A. Draeseke, G. Marschall-Schroter, R. Kuhn, B. Mack, O. Gires, C. J. Vahl, M. Schmidt-Supprian, L. J. Strobl, U. Zimber-Strobl, CD19-independent instruction of murine marginal zone B-cell development by constitutive Notch2 signaling. *Blood* **118**, 6321-6331 (2011).
51. S. A. Oracki, J. A. Walker, M. L. Hibbs, L. M. Corcoran, D. M. Tarlinton, Plasma cell development and survival. *Immunol Rev* **237**, 140-159 (2010).

Acknowledgments: We thank the animal facility of the Helmholtz Center and our animal care takers for excellent housing of the mice and Krisztina Zeller and Gabriele Marschall-Schröter for excellent technical assistance. We thank Simon Wenzl for his excellent work in the scope of his internship. We are grateful to Marina Jimenez Munoz and Hannah Busen from the Core Facility Statistical Consulting for their support with the statistical analyses. **Funding:** This work was supported by a

grant from the Sander Stiftung (2011.076.1 and .2) and the Deutsche Forschungsgemeinschaft (DFG ZI1382/4-1, SFB1243 TPA13). **Author contributions:** Contribution: S.F., L-S.: performed research, interpreted data, helped to write the manuscript; L.J.S.: analyzed and interpreted data, prepared figures; T.B., L.K., S.E., S.Fr., F.M.L.: performed research; E.H., M.B. provided mice and discussed the manuscript; B.J., G.W.B. interpreted data and discussed the manuscript, U.Z-S. designed experiments, interpreted data, wrote the manuscript. **Competing interests:** The authors declare that they have no competing interests. **Data and Materials Availability**: All data needed to evaluate the conclusions in the paper are present in the paper or the Supplementary Materials.

Figure Legends:

Fig. 1. Impaired B cell development in DKO mice. (A) Total numbers of living $B220^+$ B cells in the BM of control (WT and Mb1-Cre mice combined), *Braf* and *Raf1* single-knockout (KO) and double-knockout (DKO) mice. *N* = 6-10 mice per group. **(B)** Numbers of pro-B and early pre-B cells ($CD43^+B220^{low}$), late pre-B and immature B cells ($CD43^-B220^{low}$), as well as recirculating ($CD43^-B220^{high}$) B cells in the indicated genotypes. *N* = 5-7 mice per genotype. The gating strategy for the B cell fractions in the BM is shown in fig. S2, A and B. **(C)** Fractions A-C´ according to the classification of Hardy *et al*. (*2*). The plots are gated on living $B220^+CD43^+$ lymphocytes (pro-B and early pre-B cells). Fraction A: $BP\text{-}1^-CD24^-$; fraction B: $BP\text{-}1^-CD24^+$; fraction C: $BP\text{-}1^+CD24^{int}$; fraction C´: $BP\text{-}1^+CD24^{high}$ as labelled in the FACS plots of WT B cells. Numbers in the plots indicate means ± SD of fractions A to C´. FACS plots are representative for *N* = 6-9 mice per genotype. **(D)** The graph shows the ratio of percentages between fractions C´ and C. *N* = 6-9 mice per genotype. Dots in the graphs (A), (B) and (D) represent values from individual mice, the lines represent the means. Controls are either WT or Mb1-Cre mice. Statistics in (A), (B) and (D) were calculated with an ordinary one-way ANOVA with Dunnett's multiple comparison with * $P<0.05$, *** $P<0.001$.

Fig. 2. Reduced B cell numbers in the periphery of DKO mice. (**A**) Spleen weight and splenic B cell ($B220^+$) numbers in control (Mb1-Cre and WT mice combined), *Braf* and *Raf1* single-knockout (KO) and double-knockout (DKO) mice. *N* = 10-20 mice per genotype (splenic weight), *N* = 6-10 mice per genotype (B cell numbers). (**B**) Percentages of MZ B ($CD21^{high}CD23^{low}$) and Fo B ($CD21^{int}CD23^{high}$) cells in the spleens of mice with the indicated genotypes. The plots are gated on living $B220^+$

lymphocytes. (**C**) Total numbers of Fo B and MZ B cells in the spleens of mice with the indicated genotypes and gated as indicated in (B). Data in (B) and (C) are from *N* = 6-10 mice per genotype. (**D**) Percentages of B1a cells ($B220^{low}CD5^{+}$, red circle) in the peritoneal cavities of mice with the indicated genotypes. Plots are gated on living IgM^{+} lymphocytes. Quantitative analysis for B1a cells is shown in fig. S3C. Data are representative of *N* = 7-15 mice per genotype. Dots in (A) and (C) represent values from individual mice and the lines indicate the means. Controls are either WT or Mb1-Cre mice. Numbers in the FACS plots in (B) and (D) indicate the means ± SD of the percentages of the gated populations. Gated populations are labelled in red in the FACS plots of WT mice. Ordinary one-way ANOVA with Dunnett's multiple comparison was performed with * P<0.05, ** P<0.01, *** P<0.001, **** P<0.0001.

Fig. 3. Reduced influx and differentiation of immature B cells in DKO mice. (**A**) Percentages and cell numbers of T1 ($IgM^{high}CD23^{-}$), T2 ($IgM^{high}CD23^{+}$), and T3 ($IgM^{low}CD23^{+}$) cells in the spleen of control (WT, ctrl) and *Braf* and *Raf1* single-knockout (KO) and double-knockout (DKO) mice. The sample control FACs plot represents a WT mouse; the quantitative data include both WT and Mb1-Cre mice as the control (ctrl). The plots are gated on living $B220^{+}AA4.1^{+}$ lymphocytes. Numbers in the FACS plots indicate means +/-SD of the percentages of the gated populations. The T1, T2 and T3 cell populations are indicated in red in the FACS plot of the WT control. (**B**) Ratio of the percentages of T2 to T1 cells in mice of each genotype. Dots in the graphs from (A) and (B) represent values from individual mice, and the lines represent the means. Data in (A) and (B) are from *N* = 6-10 mice per genotype (**C**) Percentages of $BrdU^{+}$ B cells in the blood during the pulse and chase at the indicated time points and analysis of the decline in $BrdU^{+}$ cells by setting the

percentages of $BrdU^+$ cells at the end of the pulse (day 14) to 100%. The values of the different genotypes at day 42 and 70 were calculated in relation to 100% $BrdU^+$ cells at day 14. (**D**) Percentages of living (TO-PRO-3^-) B cells of the indicated genotypes cultured without or with CD40-stimulation up to 5 days. Data in (C) and (D) are from *N* = 3 independent experiments, depicting the mean of 3 mice per genotype. Each time point was analyzed separately. Brown/Forsythe and Welch one-way Anova with Dunnett's multiple comparison (A), and ordinary one-way ANOVA with Dunnett's multiple comparison (B) to (D). * P<0.05, ** P<0.01.

Fig. 4. **Impaired immune responses in DKO mice.** (**A**) Immunohistochemistry of spleens from WT, *Braf* and *Raf1* single-knockout (KO) and double-knockout (DKO) mice immunized with the TD antigen NP-CGG. Tissue was stained with PNA (blue) and an antibody specific for IgM (red) to detect germinal centers (GC) and B cell areas. n.i., non-immunized WT mice. Data are representative for *N* = 2 mice for B-Raf KO and Raf-1 KO, and *N* = 3 mice for WT and DKO; *N* = 2 . Scale bar, 100μm. (**B**) Percentages of GC B cells ($PNA^{high}CD95^{high}$) in the spleens of TD-immunized mice with the indicated genotypes. The gating strategy of GC B cells is shown in fig. S4. *N* = 10-11 immunized mice per genotype and *N* = 3 n.i. WT mice. (**C**) Relative titers of NP-specific IgM, total IgG1 (NP16-specific), and high-affinity (NP4-specific) IgG1 antibodies in the serum of TD-immunized mice of the indicated genotypes. *N* = 7-10 immunized mice per genotype and N = 6 n.i. WT mice. Data points in (B) and (C) represent values from individual mice, and the lines represent the means. (**D**) Percentages of plasmablasts ($IRF4^{high}CD138^{high}$) in n.i. WT and mice of the indicated genotypes immunized with the TI antigen NP-LPS. (**E**) Quantification of the indicated types of antibody-secreting cells (ASCs) in splenic cells isolated from TI-immunized

mice with the indicated genotypes. The data points represent the numbers of cells (spots in ELISpot assay) that secrete NP-specific antibodies among $5x10^5$ splenic cells. (**F**) Relative serum titers of NP-specific antibodies in TI-immunized mice of the indicated isotypes. Data in (D) to (F) represent values from individual mice (*N* = 3 n.i. WT mice, *N* = 5 immunized WT and *N* = 6 immunized DKO mice), and the bars represent the means. Statistical analysis of the relative serum titers (C) and (F) was performed after logarithmic transformation due to a lognormal distribution of the values. Ordinary one-way ANOVA with Dunnett's multiple comparison was performed in (B) and (C). Ordinary one-way ANOVA with Sidak's multiple comparison was performed in (D) to (F). Brown/Forsythe and Welch one-way ANOVA was used to calculate the statistics for NP IgM in (C) and NP IgG3 titers in (F). * P<0.05, ** P<0.01, *** P<0.001, **** P<0.0001.

Fig. 5. Impaired plasma cell differentiation of DKO B cells. (**A**) Illustration of the markers that increase and decrease during PC differentiation based on (*51*). (**B to H**) Isolated splenic B cells of control (WT or Mb1-Cre mice) and *Braf1* and *Raf1* DKO mice were cultured for 3 days with LPS. All FACS plots were gated on living cells. Percentages of PB ($CD138^{high}B220^{low}$) cells in the cultures were quantified (B) using the gating strategy shown in fig. S5A. WT and Mb1-Cre mice are controls. Ctrl, data from WT and MB1-Cre mice combined. N = 15 mice per genotype. Percentages of $BLIMP1^+$ B lymphocytes (C) and PB ($CD138^{high}B220^{low}$) cells among the living $BLIMP1^+$ cells (D) were quantified. *N* = 6 mice per genotype (C) and (D). IRF4 and PAX5 staining was performed on isolated cells at day 0 (d0) and at day 3 (d3) of LPS stimulation, and the numbers of $IRF4^{high}PAX5^{low}$ cells were quantified (E). Percentages of pre-PB ($IRF4^{high}PAX5^{low}CD138^{int}B220^+$) and PB

(IRF4^{high}PAX5^{low}CD138^{high}B220^{low}) cells within the B cell population were quantified using the gating strategy shown in fig. S5C (F). *N* =10 mice per genotype were analyzed in (E) and (F), controls (ctrl) are Mb1-Cre and WT mice. CFSE staining was performed to determine cell proliferation. An overlay of the CFSE staining at day 1 and day 3 of LPS stimulation is shown (G). Percentages of PB in each cell division were quantified using the gating strategy shown in fig. S5D to monitor CD138^{high}B220^{low} cells at each cell division (H). *N* = 3 mice per genotype were analyzed in (G) and (H). For all panels, data points in graphs represent values from individual mice, and bars represent the means ±S D. Statistical analyses in (C), (E), and (F) were performed after logarithmic transformation due to a lognormal distribution of the values. Unpaired Student's t test [(B) to (E) and (H)] and two-way ANOVA with Sidak's multiple comparison (F). * P<0.05, ** P<0.01, *** P<0.001, **** P<0.0001.

Fig. 6. Increased ERK phosphorylation in DKO B cells. (**A**) Splenic B cells from control (WT and Mb-1-Cre mice combined) and *Braf1* and *Raf1* DKO mice were stimulated with LPS, and amounts of pERK at the indicated time points were determined in living B220^{+} lymphocytes by FACS. The graph shows means ±SD of the median fluorescence intensities (MFI) of independent samples from *N* = 11 control, N = 12 DKO mice. A representative histogram shows pERK amounts in the indicated genotypes and time points. (**B and C**) Splenic B cells from control (Mb1-Cre) and DKO mice were stimulated with LPS for the indicated amounts of time (B) or stimulated with an IgM-specific antibody (anti-IgM) (C). MEK, pMEK, pERK, ERK, and Tubulin were detected by Western blotting. Quantitative data are shown in fig. S6, A and B. *N* = 3 (B) and *N* = 5 (C) independent samples for genotype and

condition. (**D**) Splenic B cells from control (Mb1-Cre) and DKO mice were stimulated with LPS for the indicated amounts of time, and nuclear pERK was quantified. Amounts of pERK were normalized to the loading control, LaminB2. The values of unstimulated Mb1-Cre (control) and DKO B cells are depicted with dotted lines. Means ±SD were calculated from *N* = 3 independent samples per genotype. (**E**) Basal amounts of pERK in FoB ($CD21^{int}CD23^{+}$) and MZ B ($CD21^{high}CD23^{low}$) cells from control (Mb1-Cre) and DKO mice were analyzed by FACS. The histograms are gated on living $B220^{+}$ lymphocytes. *N* = 4 mice per genotype (**F**) Basal amounts of pERK in recirculating BM B cells ($B220^{high}CD43^{-}$) in control and DKO mice were determined by FACS. (**G**) Means ±SD of the MFIs of pERK amounts in the indicated B cell populations of the BM: pro-B cells ($B220^{+}CD43^{+}CD25^{-}$), early pre-B ($B220^{+}CD43^{+}CD25^{+}$), late pre-B ($B220^{+}CD43^{-}CD25^{+}$), immature ($B220^{+}CD43^{-}CD25^{-}$), and recirculating ($B220^{high}CD43^{-}$) B cells. The dotted lines indicate the values of the isotype controls. (F) and (G) *N* = 10 mice per genotype. To differentiate non-specific background from specific antibody signals we used an isotype control (Iso) in (A), (E), (F) and (G). All samples were stained in parallel with an antibody matching the class and type of the pERK antibody but lacking the specificity of pERK. Ordinary two-way ANOVA with Tukey's in (A) and (G), or Sidak's in (D) and (E) multiple comparison. * P<0.05, ** P<0.01, **** P<0.0001.

Fig. 7. RAF-independent ERK phosphorylation in mature B cells. (**A to E**) B cells from control (WT or MB1-Cre mice) and DKO mice were treated either with vehicle (DMSO) or the chemical inhibitors LY30 (pan-RAF inhibitor LY3009120), iSYK (SYK inhibitor p505-15), iAKT (AKT inhibitor AKTi-1/2), LY29 (PI3K-inhibitor LY294002), or iPAK (PAK-inhibitor PF-3758309) as indicated. Amounts of pERK1

and pERK2 in lysates from untreated (us) or LY30-treated B cells compared to DMSO-treated controls were quantified from immunoblots and are shown as means ±SD of the fold induction of pERK1 and pERK2 (A). Western blotting for the indicated proteins was performed with lysates from splenic B cells treated with DMSO or LY30 (B), iSYK or iAKT (C), LY29 (D), or iPAK (E) before they were stimulated with an IgM-specfic antibody. Tubulin is a loading control. Numbers of independent samples: For (A), *N* = 6 mice per genotype for untreated cells, and *N* = 6 control (WT and Mb1-Cre combined) mice and *N* = 4 DKO mice for Ly30-treated cells. For (B), *N* = 3 Mb1-Cre mice and *N* =2 DKO mice. For (C), *N* = 2 per genotype per treatment. For (D and E), *N* = 3 mice per genotype per treatment. Numbers below the pERK blots in (B) show the amounts of pErk1 and pErk2 relative to the unstimulated and uninhibited values (set to 1) after normalization to Tubulin. Quantifications of the Western Blots from (C) to (E) are shown in fig. S9 A to C. Two-way ANOVA with Sidak's multiple comparison was performed in (A). Statistical analysis was performed after logarithmic transformation due to a lognormal distribution of the values. * $P<0.05$, ** $P<0.01$.

Fig. 8. Diminished ERK phosphorylation in pre-PBs from B cells of DKO mice. (**A**) PAX5 and IRF4 staining of isolated splenic naïve B cells ($IRF4^{low}PAX5^{high}$) and LPS-stimulated splenic B cells (3 days) from Mb1-Cre and DKO mice. Naïve B cells represent ex vivo isolated B cells that were stained before cells were stimulated with LPS. LPS-stimulated B cells were further subdivided into activated (act.) B cells ($IRF4^{med}PAX5^{high}$), and pre-PBs and PBs ($IRF4^{high}PAX5^{low}$). The FACS plots are gated on living lymphocytes. (**B**) The $IRF4^{high}PAX5^{low}$ population was further subdivided into pre-PB ($CD138^{low}B220^{+}$) and PB ($CD138^{high}B220^{low}$) populations.

The FACS plots are gated on live IRF4^{high}PAX5^{low} cells. (**C**) Representative overlays of pERK or ERK abundance in the naïve B cell, activated B cell, pre-PB, and PB subpopulations. (**D**) Fold inductions of pERK and ERK in the indicated subpopulations relative to naive B cells. (**E**) Ratios of the MFIs of pERK to ERK for each indicated subpopulation within one mouse. (A) to (E) *N* = 5 control mice, *N* = 4 DKO mice. Control mice are Mb1-Cre or WT mice combined. Ordinary two-way ANOVA with Tukey's (D) or Sidak's (E) multiple comparison was performed. **** P<0.0001. (**F**) Hypothetical signaling scheme for MEK-ERK activation in naïve and activated B cells compared to PCs.

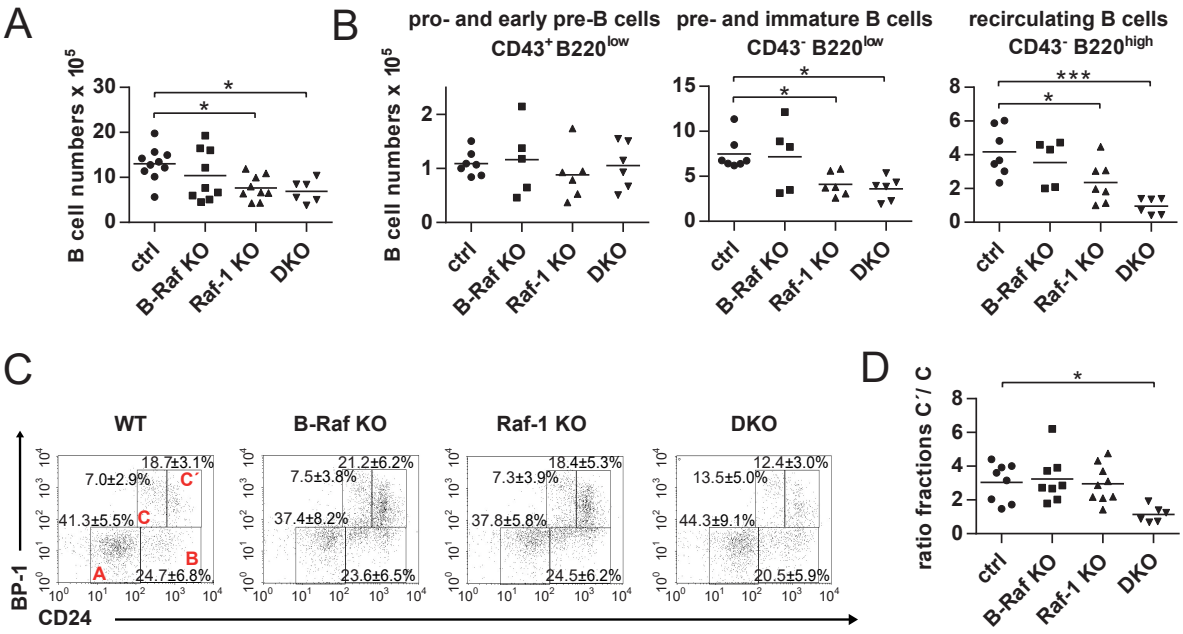
A
B cell numbers x 10^5
ctrl
B-Raf KO
Raf-1 KO
DKO
B
pro- and early pre-B cells
CD43+ B220low
pre- and immature B cells
CD43- B220low
recirculating B cells
CD43- B220high
C
WT
B-Raf KO
Raf-1 KO
DKO
BP-1
CD24
18.7±3.1%
7.0±2.9%
41.3±5.5%
24.7±6.8%
21.2±6.2%
7.5±3.8%
37.4±8.2%
23.6±6.5%
18.4±5.3%
7.3±3.9%
37.8±5.8%
24.5±6.2%
12.4±3.0%
13.5±5.0%
44.3±9.1%
20.5±5.9%
D
ratio fractions C´/ C

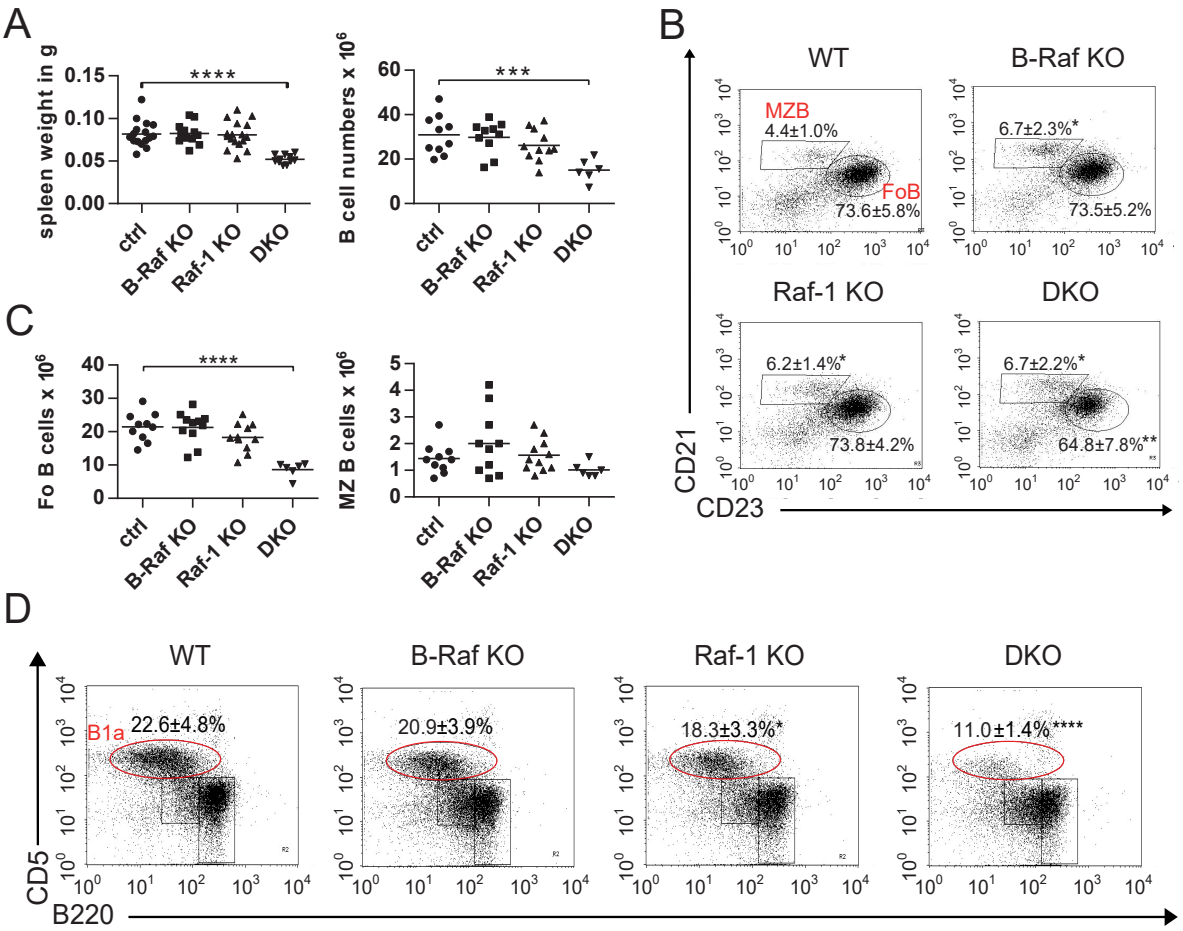
A
spleen weight in g
0.15
0.10
0.05
0.00
****
ctrl
B-Raf KO
Raf-1 KO
DKO
B cell numbers x 10^6
60
40
20
0
***
B
WT
B-Raf KO
MZB
4.4±1.0%
FoB
73.6±5.8%
6.7±2.3%*
73.5±5.2%
Raf-1 KO
DKO
6.2±1.4%*
73.8±4.2%
6.7±2.2%*
64.8±7.8%**
CD21
CD23
C
Fo B cells x 10^6
40
30
20
10
0
****
MZ B cells x 10^6
5
4
3
2
1
0
D
WT
B-Raf KO
Raf-1 KO
DKO
B1a
22.6±4.8%
20.9±3.9%
18.3±3.3%*
11.0±1.4%****
CD5
B220

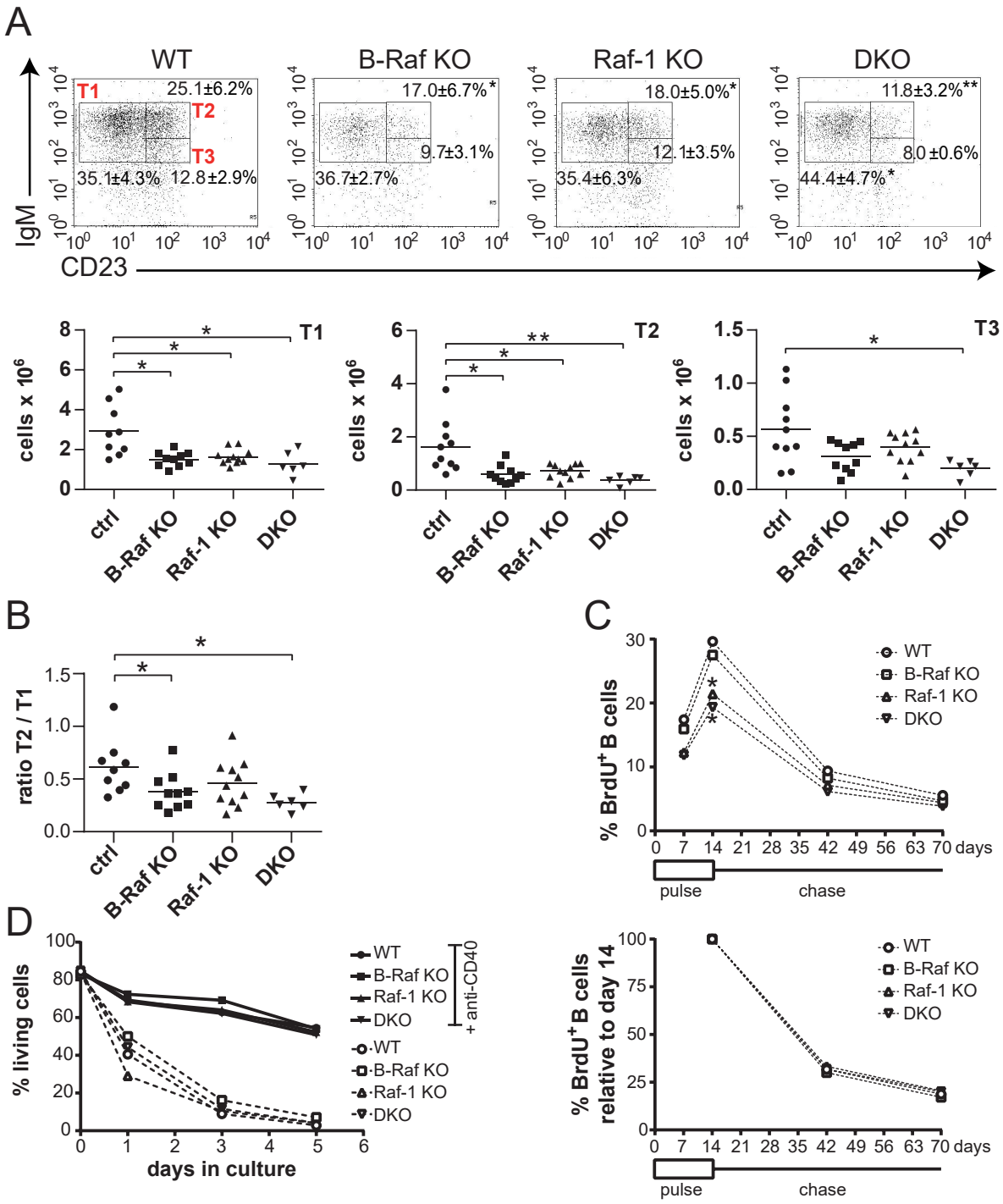
A
WT
B-Raf KO
Raf-1 KO
DKO
T1
T2
T3
25.1±6.2%
35.1±4.3%
12.8±2.9%
17.0±6.7%*
9.7±3.1%
36.7±2.7%
18.0±5.0%*
12.1±3.5%
35.4±6.3%
11.8±3.2%**
8.0 ±0.6%
44.4±4.7%*
IgM
CD23
cells x 10^6
ctrl
B-Raf KO
Raf-1 KO
DKO
B
ratio T2 / T1
C
% BrdU+ B cells
WT
B-Raf KO
Raf-1 KO
DKO
pulse
chase
days
D
% living cells
days in culture
+ anti-CD40
% BrdU+ B cells relative to day 14

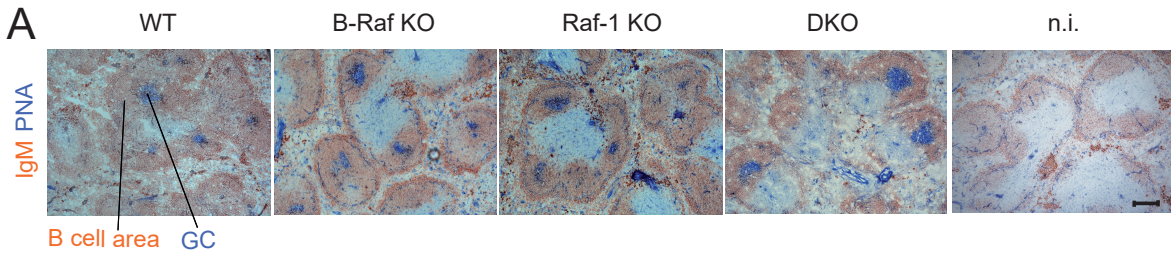
A
WT
B-Raf KO
Raf-1 KO
DKO
n.i.
IgM PNA
B cell area
GC

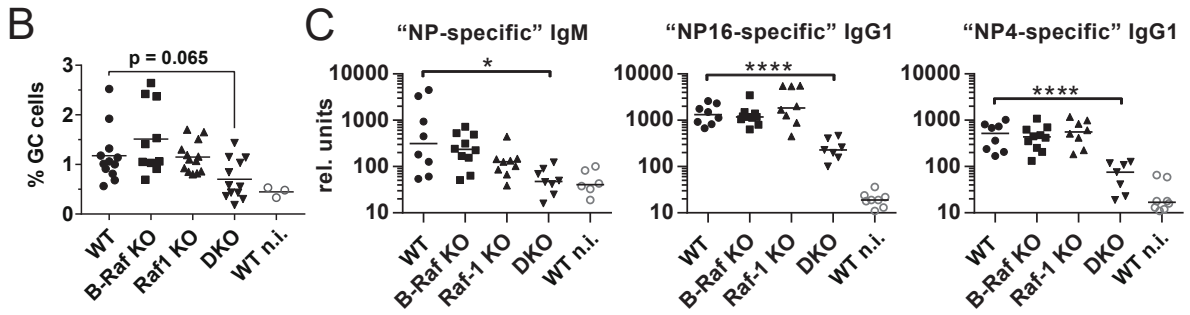
B
p = 0.065
% GC cells
WT
B-Raf KO
Raf1 KO
DKO
WT n.i.
C
"NP-specific" IgM
"NP16-specific" IgG1
"NP4-specific" IgG1
rel. units
WT
B-Raf KO
Raf-1 KO
DKO
WT n.i.

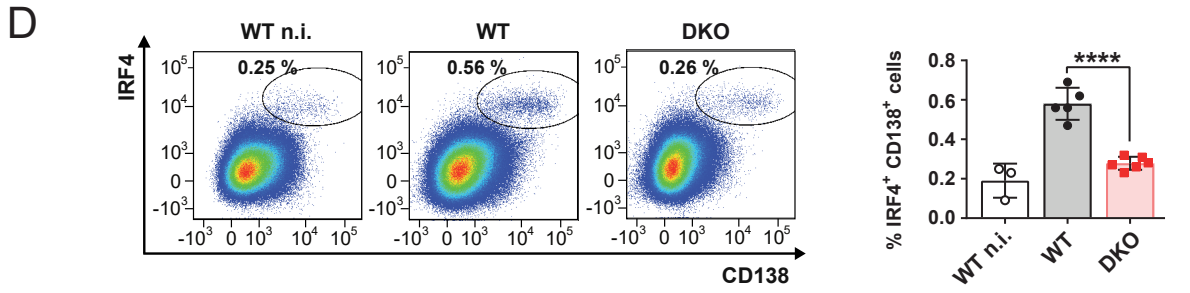
D
WT n.i.
WT
DKO
IRF4
CD138
0.25 %
0.56 %
0.26 %
% IRF4+ CD138+ cells
WT n.i.
WT
DKO

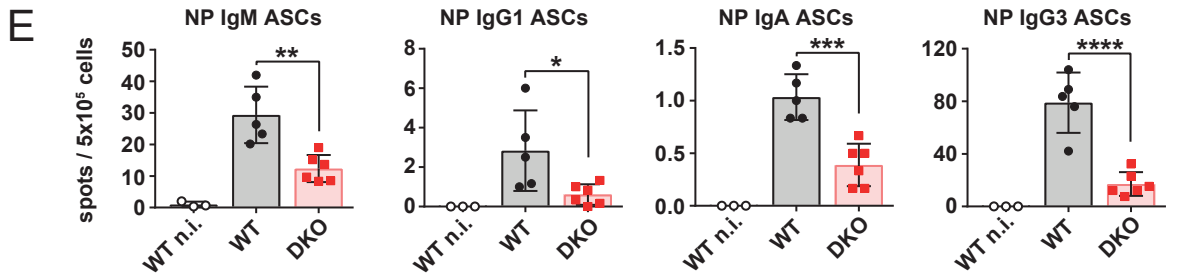
E
NP IgM ASCs
NP IgG1 ASCs
NP IgA ASCs
NP IgG3 ASCs
spots / 5x10⁵ cells
WT n.i.
WT
DKO

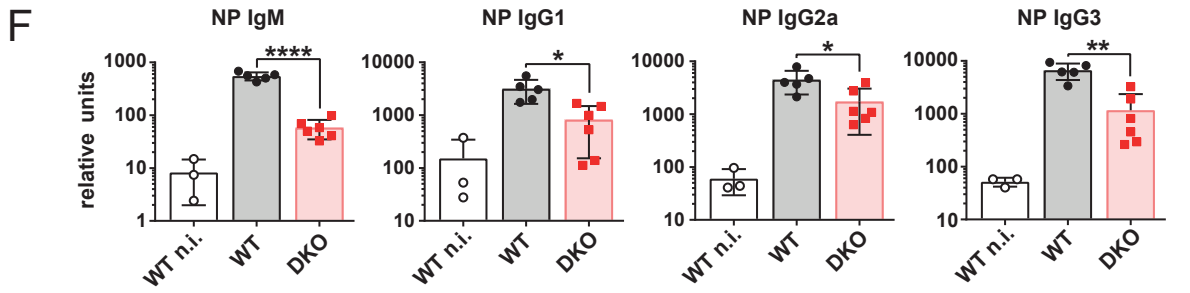
F
NP IgM
NP IgG1
NP IgG2a
NP IgG3
relative units
WT n.i.
WT
DKO

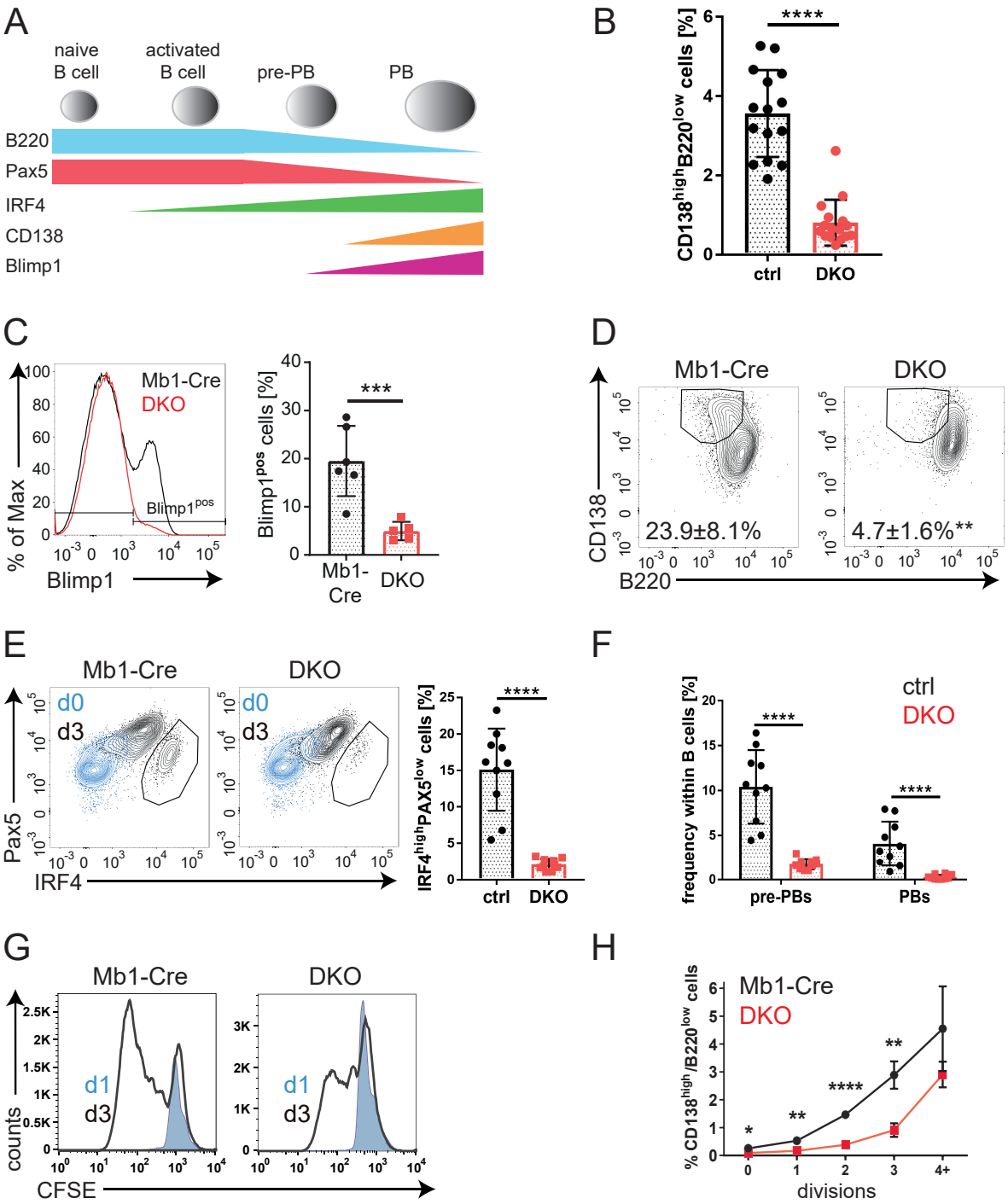
A
naive B cell
activated B cell
pre-PB
PB
B220
Pax5
IRF4
CD138
Blimp1
B
CD138highB220low cells [%]
****
ctrl
DKO
C
Mb1-Cre
DKO
% of Max
Blimp1
Blimp1pos
Blimp1pos cells [%]
***
Mb1-Cre
DKO
D
Mb1-Cre
DKO
CD138
B220
23.9±8.1%
4.7±1.6%**
E
Mb1-Cre
DKO
d0
d3
Pax5
IRF4
IRF4highPAX5low cells [%]
****
ctrl
DKO
F
ctrl
DKO
frequency within B cells [%]
****
****
pre-PBs
PBs
G
Mb1-Cre
DKO
d1
d3
counts
CFSE
H
Mb1-Cre
DKO
% CD138high/B220low cells
*
**
****
**
divisions

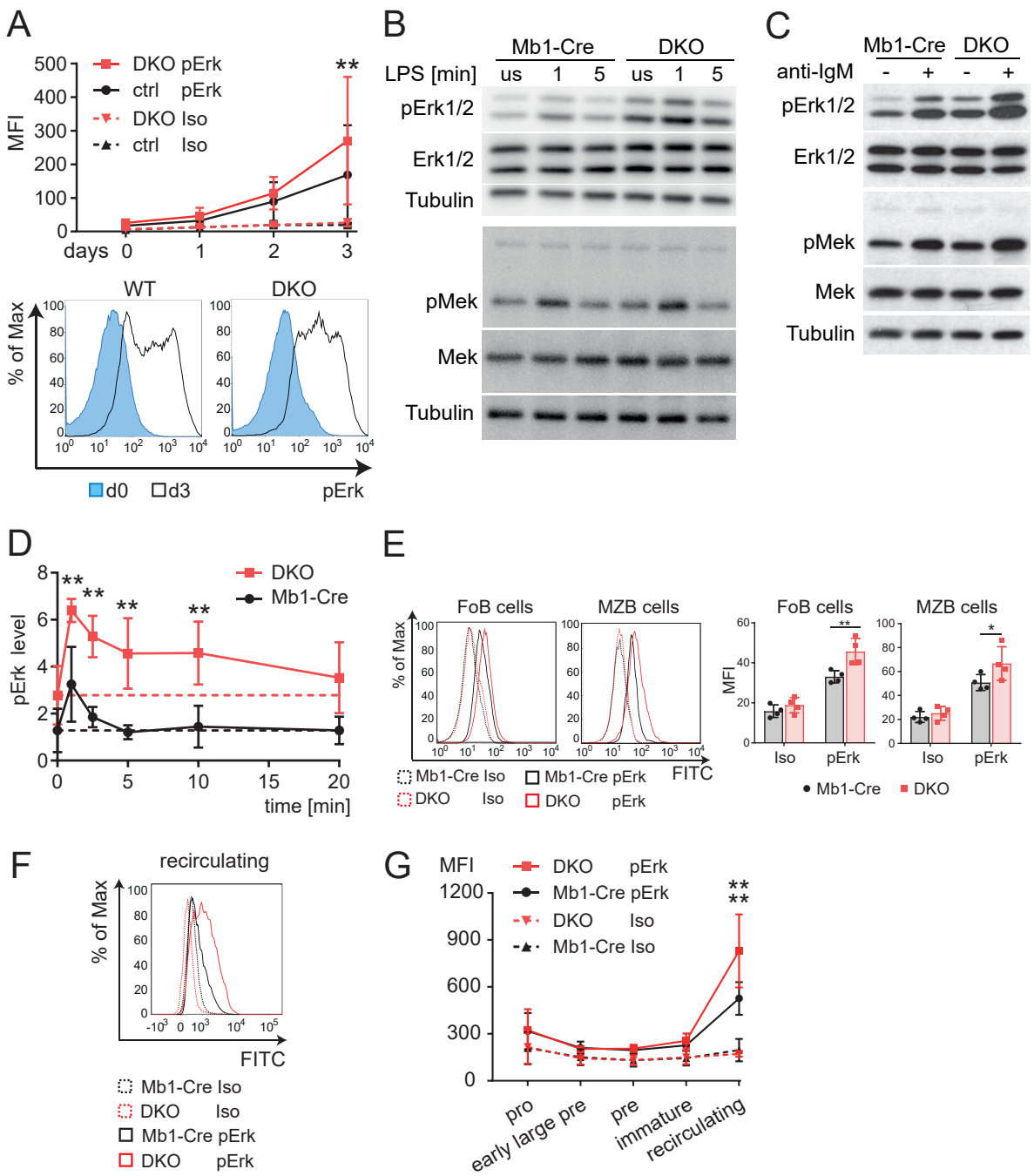
A
MFI
DKO pErk
ctrl pErk
DKO Iso
ctrl Iso
days 0 1 2 3
WT
DKO
% of Max
d0 d3
pErk
B
Mb1-Cre
DKO
LPS [min]
us 1 5 us 1 5
pErk1/2
Erk1/2
Tubulin
pMek
Mek
Tubulin
C
Mb1-Cre DKO
anti-IgM - + - +
pErk1/2
Erk1/2
pMek
Mek
Tubulin
D
DKO
Mb1-Cre
pErk level
time [min]
E
FoB cells
MZB cells
% of Max
Mb1-Cre Iso
DKO Iso
Mb1-Cre pErk
DKO pErk
FITC
MFI
Iso
pErk
Mb1-Cre
DKO
F
recirculating
% of Max
FITC
Mb1-Cre Iso
DKO Iso
Mb1-Cre pErk
DKO pErk
G
MFI
DKO pErk
Mb1-Cre pErk
DKO Iso
Mb1-Cre Iso
pro
early large pre
pre
immature
recirculating

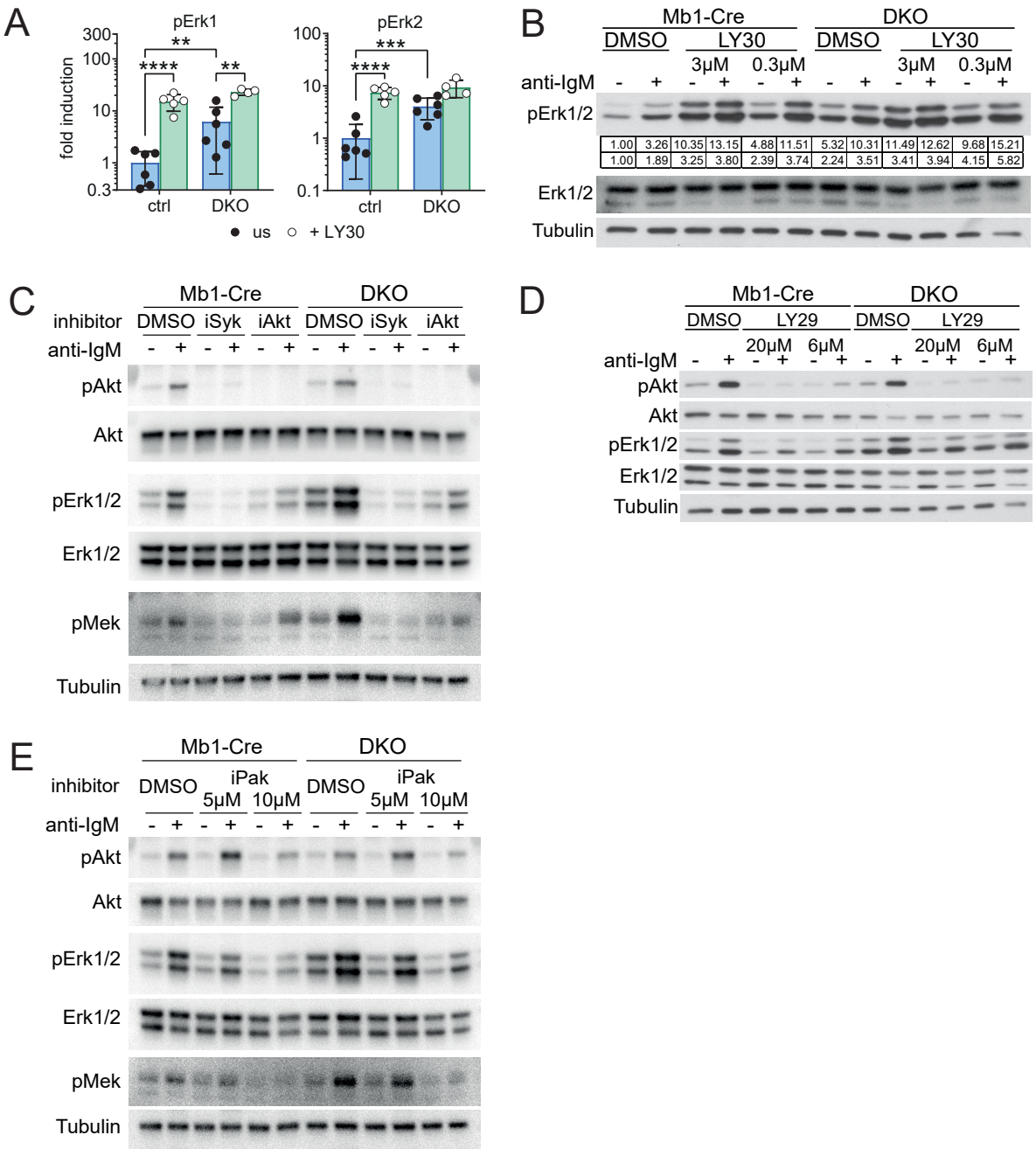
A
pErk1
pErk2
fold induction
300
100
10
1
0.3
100
10
1
0.1
**
****
**
***
****
ctrl
DKO
ctrl
DKO
us
+ LY30
B
Mb1-Cre
DKO
DMSO
LY30
DMSO
LY30
3μM
0.3μM
3μM
0.3μM
anti-IgM
pErk1/2
1.00 3.26 10.35 13.15 4.88 11.51 5.32 10.31 11.49 12.62 9.68 15.21
1.00 1.89 3.25 3.80 2.39 3.74 2.24 3.51 3.41 3.94 4.15 5.82
Erk1/2
Tubulin
C
Mb1-Cre
DKO
inhibitor
DMSO
iSyk
iAkt
DMSO
iSyk
iAkt
anti-IgM
pAkt
Akt
pErk1/2
Erk1/2
pMek
Tubulin
D
Mb1-Cre
DKO
DMSO
LY29
DMSO
LY29
20μM
6μM
20μM
6μM
anti-IgM
pAkt
Akt
pErk1/2
Erk1/2
Tubulin
E
Mb1-Cre
DKO
inhibitor
DMSO
iPak
5μM
10μM
DMSO
iPak
5μM
10μM
anti-IgM
pAkt
Akt
pErk1/2
Erk1/2
pMek
Tubulin

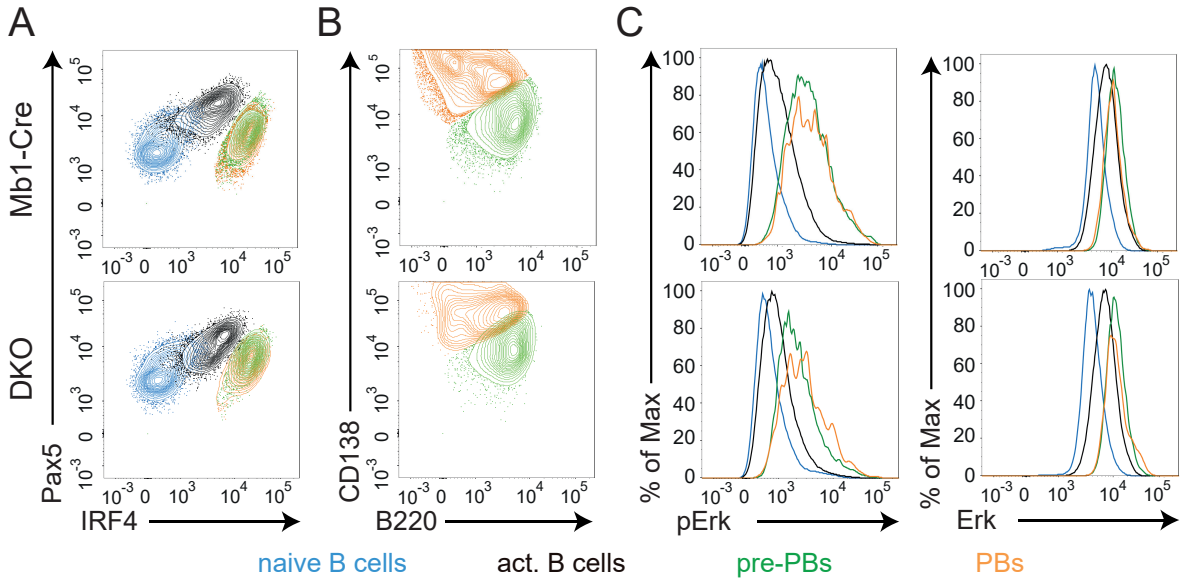
A
B
C
Mb1-Cre
DKO
Pax5
IRF4
CD138
B220
% of Max
pErk
Erk
naive B cells
act. B cells
pre-PBs
PBs

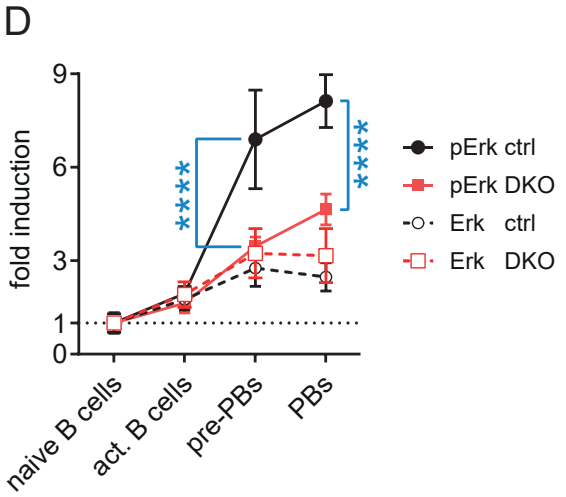
D
fold induction
pErk ctrl
pErk DKO
Erk ctrl
Erk DKO
naive B cells
act. B cells
pre-PBs
PBs

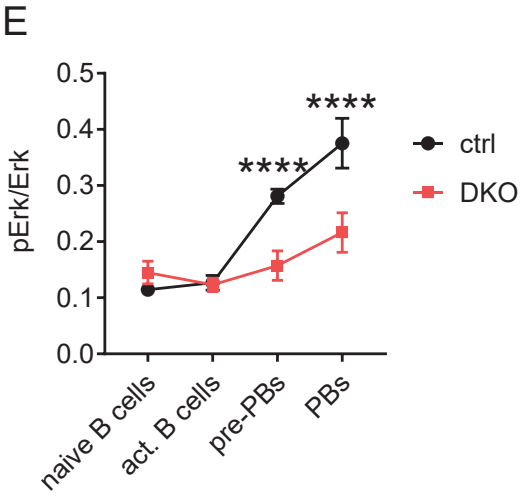
E
pErk/Erk
ctrl
DKO
naive B cells
act. B cells
pre-PBs
PBs

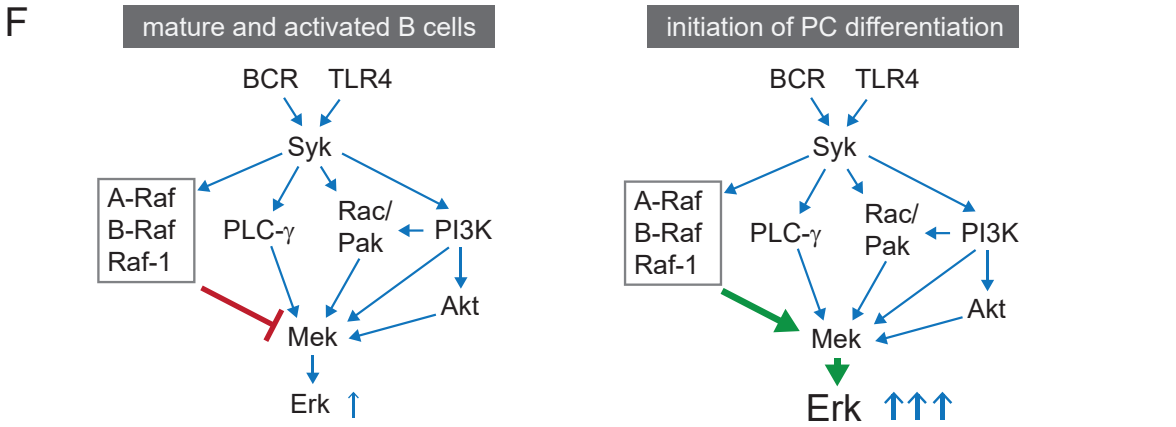
F
mature and activated B cells
initiation of PC differentiation
BCR
TLR4
Syk
A-Raf
B-Raf
Raf-1
PLC-γ
Rac/
Pak
PI3K
Akt
Mek
Erk

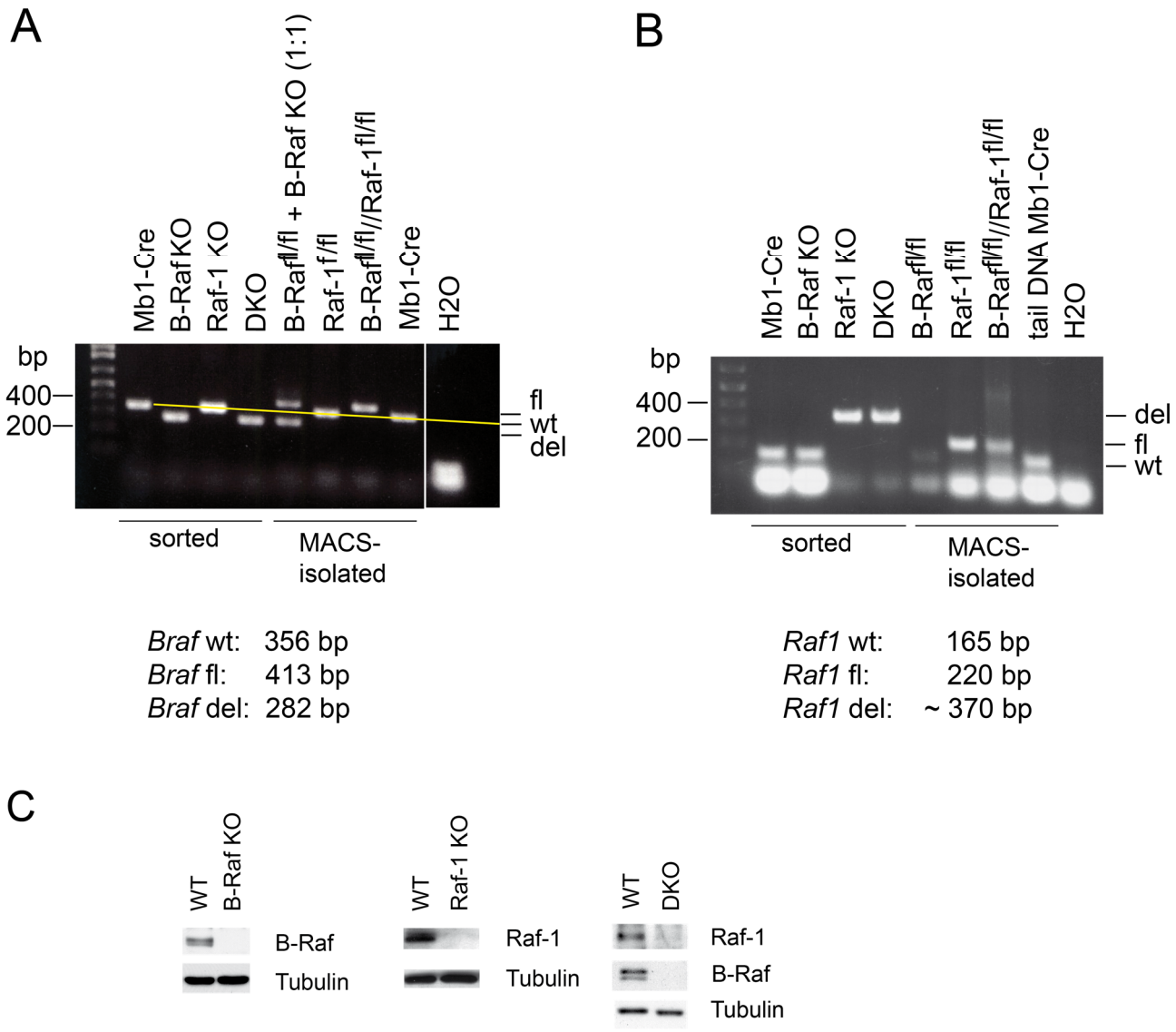

Fig. S1. Deletion of *Braf* and *Raf1* in B cells from SKO and DKO mice. (**A-B**) The loxP-flanked regions were amplified by PCR from DNAs prepared from $B220^{+}CD19^{+}$-sorted or CD43-depleted (MACS) splenic B cells from *Raf1*$^{fl/fl}$//*Mb1-cre* (Raf-1 KO), *Braf*$^{fl/fl}$//*Mb1-cre* (B-Raf KO) or *Braf*$^{fl/fl}$//*Raf1*$^{fl/fl}$//*Mb1-cre* (DKO) mice. The expected fragment sizes are indicated: wild-type locus (wt), recombinant floxed allele (fl), recombinant deleted allele (del). Bands of the wt allele are connected by a yellow line. Data are representative of 3 independent experiments. (**C**) Western blotting for B-Raf and Raf-1 in lysates of B cells isolated from mice of the indicated genotypes. Western blots were incubated with antibodies recognizing the N-terminal part of B-Raf and the CR2 region of Raf-1 as indicated. Data are representative of 3 independent experiments.

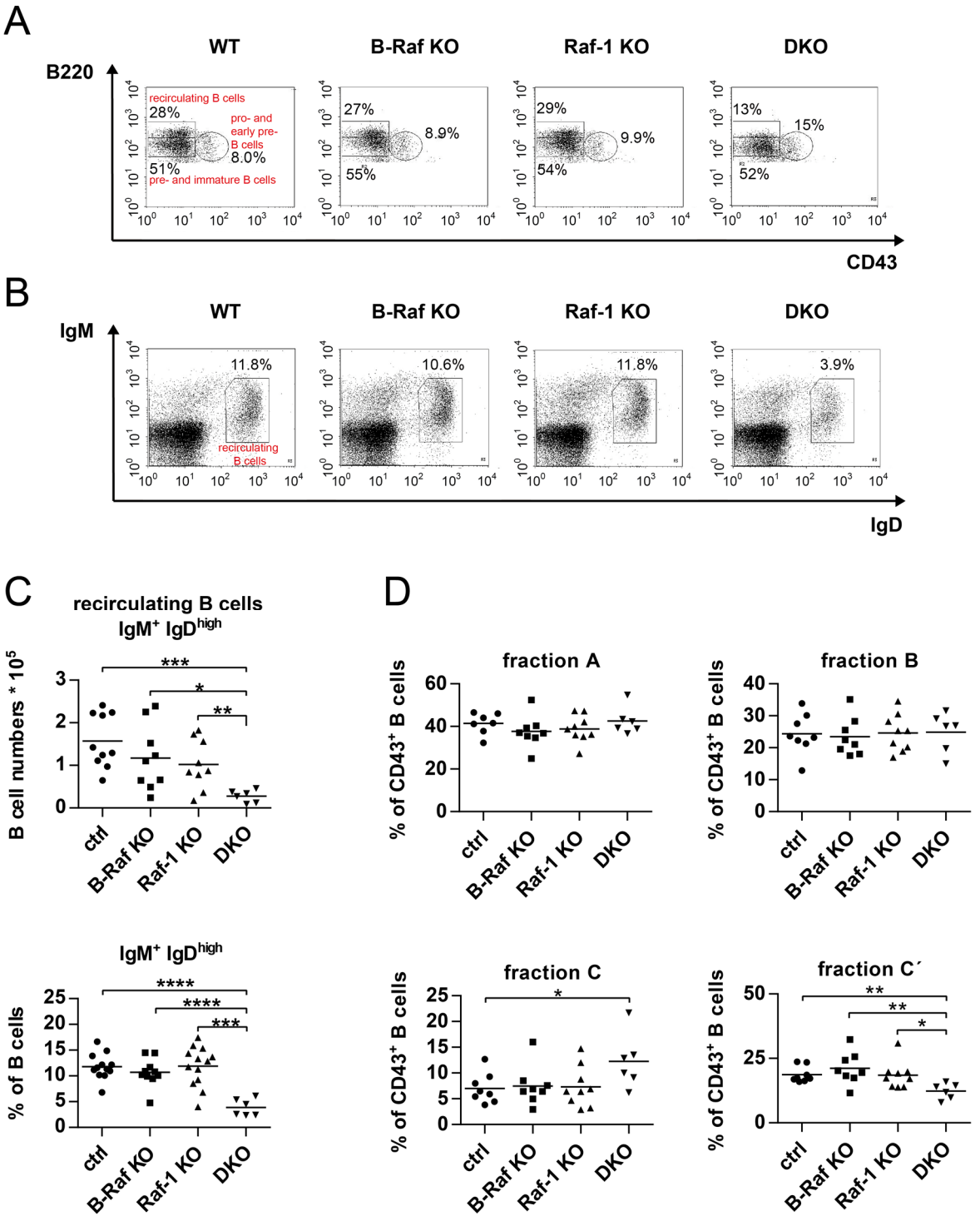

Fig. S2. B cell subpopulations in the BM (**A**) Gating strategy to determine the pro-B and early pre-B ($CD43^+B220^{low}$) cells, late pre-B and immature B ($CD43^-B220^{low}$) cells, and recirculating ($CD43^-B220^{high}$) B cells from control (WT or Mb1-Cre), B-Raf KO, Raf-1 KO, and double KO (DKO) mice in the BM. The plots are pre-gated on living $B220^+$ lymphocytes. (**B**) Representative FACS plots of recirculating (IgM^+IgD^+) B cells are shown. The FACS plots are pre-gated on living $B220^+$ lymphocytes in the BM. (**C**) Percentages and total numbers of recirculating B cells gated as in (B). (**D**) Percentages of Hardy's fractions A, B, C, and C´ gated as in Fig. 1B. Dots in (C) and (D) represent values from individual mice, the means are indicated by lines. Data in (A) to (C) are representative for N = 6-10 mice per genotype, in (D) for N = 6-8 mice per genotype. Ordinary one-way ANOVA with Dunnett's multiple comparison. * P<0.05, ** P<0.01, *** P<0.001, **** P<0.0001.

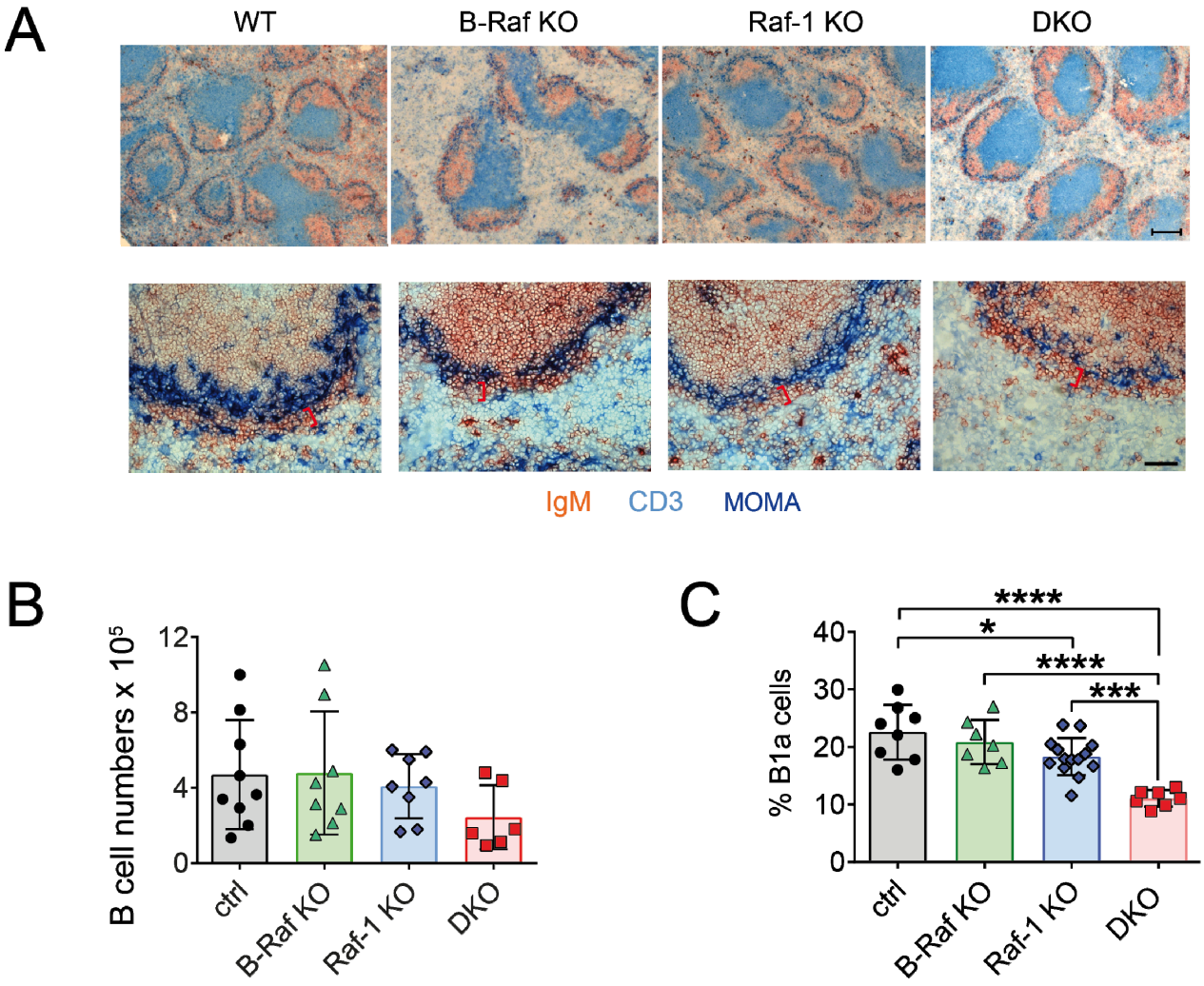

Fig. S3. Mature B cells in the periphery. (**A**) Representative cryosections of spleens from WT, B-Raf KO, Raf-1 KO, and DKO mice stained for CD3 to detect T cells (light blue), for IgM (red) to detect B cells, and for Moma-1 (dark blue) to visualize marginal-zone macrophages. The marginal zone B cell area is indicated in the higher magnifications images with red brackets. Scale bars, 200 µm (top) and 30 µm (bottom). Images are representative for $N = 2$ (B-RAF KO and RAF-1 KO mice) or $N = 3$ (WT and DKO mice) independent samples per genotype (**B**) B cell numbers (TOPRO-3$^-$, B220$^+$ lymphocytes) in the inguinal lymph nodes of the indicated genotypes. B cell numbers were calculated for one inguinal lymph node. Dots represent values from individual mice, $N = 6–8$ mice per group. (**C**) The graph shows percentages of B1a cells in the peritoneal cavity of mice of the indicated genotypes. Dots represent values from individual mice, $N = 7$-15 mice per group. In (B) and (C), controls are WT or Mb1-Cre mice. B cell numbers in (B) were logarithmic transformed due to a lognormal distribution of the values. (B) and (C) Ordinary one-way ANOVA with Tukey´s multiple comparison. * P<0.05, *** P<0.001, **** P<0.0001.

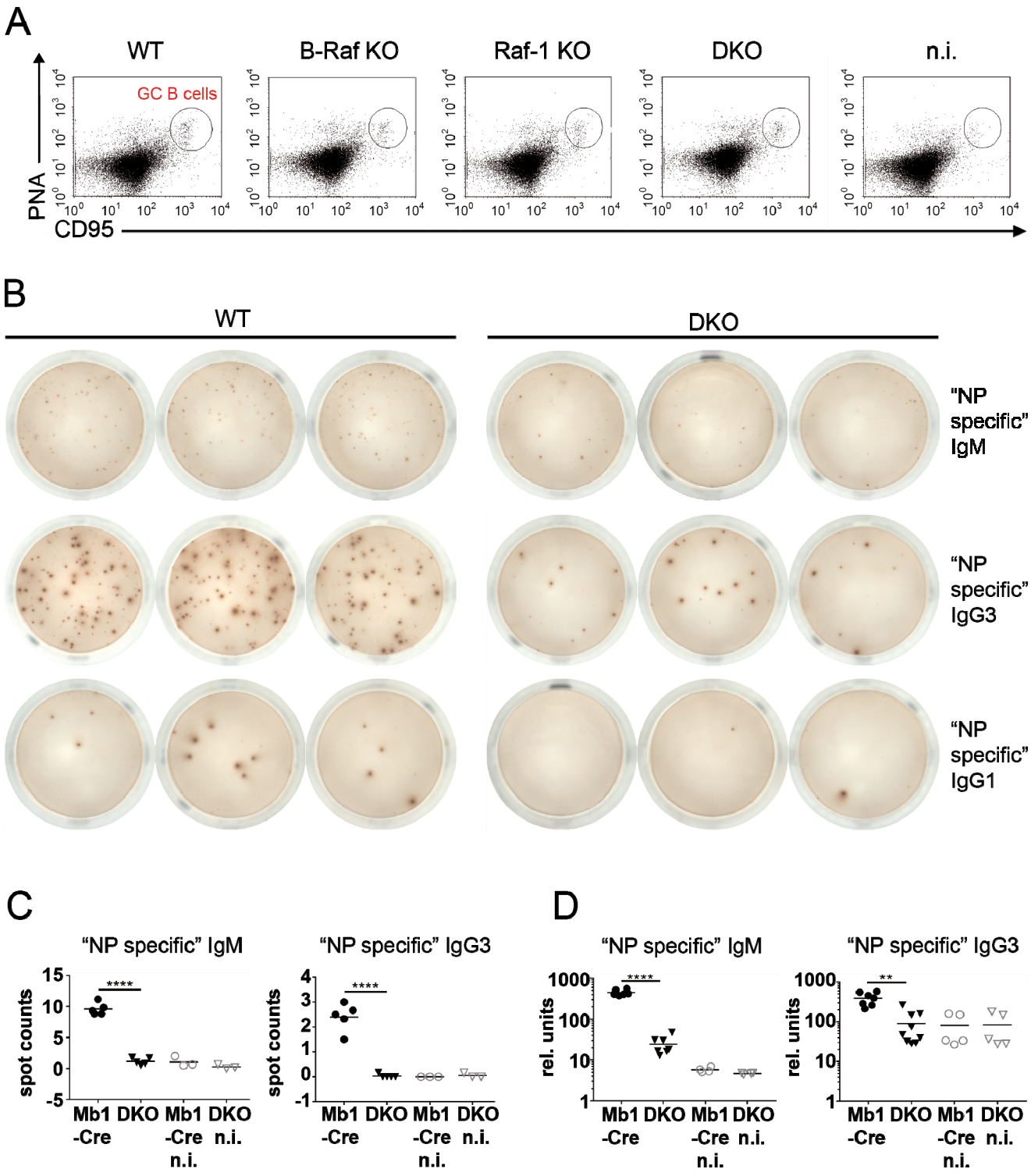
A
WT
B-Raf KO
Raf-1 KO
DKO
n.i.
GC B cells
PNA
CD95
B
WT
DKO
"NP specific" IgM
"NP specific" IgG3
"NP specific" IgG1
C
"NP specific" IgM
"NP specific" IgG3
spot counts
Mb1 -Cre
DKO
Mb1 -Cre n.i.
DKO n.i.
****
D
"NP specific" IgM
"NP specific" IgG3
rel. units
****
**

Fig. S4. **TD and TI immune responses of RAF-deficient mice. (A)** Gating strategy of germinal center B cells ($PNA^{high}CD95^{high}$) of immunized DKO and immunized and non-immunized (n.i.) WT mice (14 days p.i. with NP-CGG). Plots are gated on living $B220^{+}$ lymphocytes. (**B**) ELIspot analyses to detect NP-specific ASCs with the indicated isotypes among $5x10^5$ splenic B cells from DKO and WT mice 7 days p.i. with NP-LPS. Data are representative for $N = 5$ immunized WT and $N = 6$ immunized DKO mice. (**C and D**) Analysis of mice 14 days after immunization with NP-Ficoll. NP-specific IgM and IgG3 antibody secreting cells (ASC) were determined by ELISpot, and the numbers correspond to spots in $5x10^5$ (IgM) and $1x10^6$ (IgG3) seeded splenocytes (C). Relative serum titers of NP-specific IgM and IgG3 antibodies (D). Dots in (C) and (D) represent values from individual mice.The lines represent the means. $N = 5$ immunized and $N \geq 3$ unimmunized mice per genotype. Statistical analysis of the relative serum titers was performed after logarithmic transformation due to a lognormal distribution of the values. (C) and (D) Two-way ANOVA with Tukey's multiple comparison. ** $P<0.01$, **** $P<0.0001$.

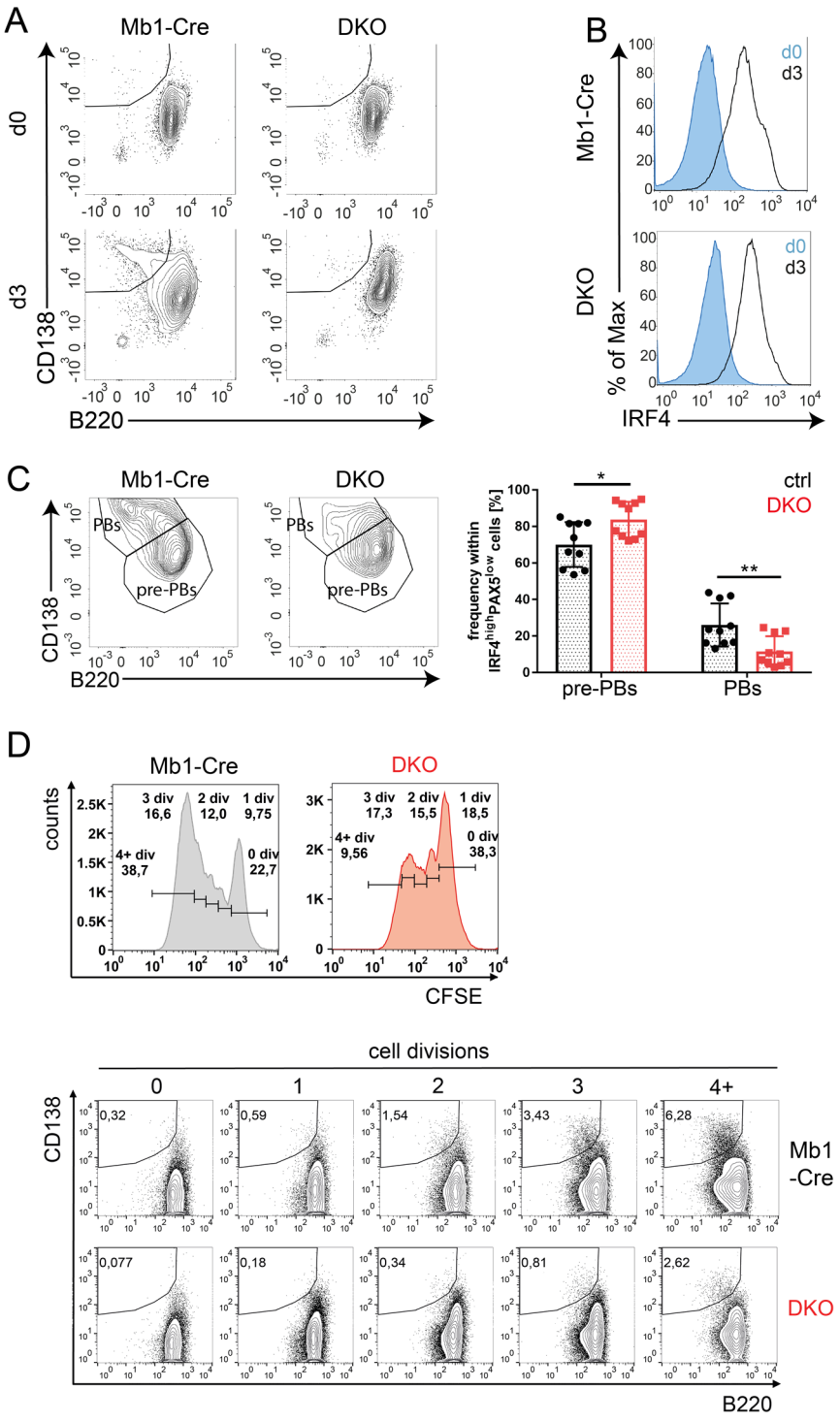

Fig. S5. Plasma cell differentiation upon LPS stimulation in vitro. (**A**) Gating strategy for PBs ($CD138^{high}B220^{low}$) without stimulation at day 0 (d0) and after three days of LPS stimulation (d3). Data are representative for $N = 15$ mice per genotype. (**B**) Representative overlays of the IRF4 amounts in unstimulated (d0) and LPS-stimulated (d3) B cells from Mb1-Cre and DKO mice. Data are representative for $N = 6$ mice per genotype (**C**). Gating and percentages of pre-PBs ($CD138^{int}B220^{+}$) and PBs ($CD138^{high}B220^{low}$) within living $IRF4^{high}PAX5^{low}$ cells (see Fig. 5E for gating). $N = 10$ mice per genotype. Controls were Mb1-Cre or WT mice. Statistics was calculated with a two-way ANOVA with Sidak's multiple comparison. * $P<0.05$, ** $P<0.01$. (**D**) Gating strategy of cell divisions (histogram). Percentages of PB ($CD138^{high}B220^{low}$) in each cell division (dot plots). The plots are gated on undivided cells (0 div) or cells with 1 division (1 div), 2 divisions (2 div), 3 divisions (3 div), and 4 or more divisions (4+ div). Data are representative for three independent experiments.

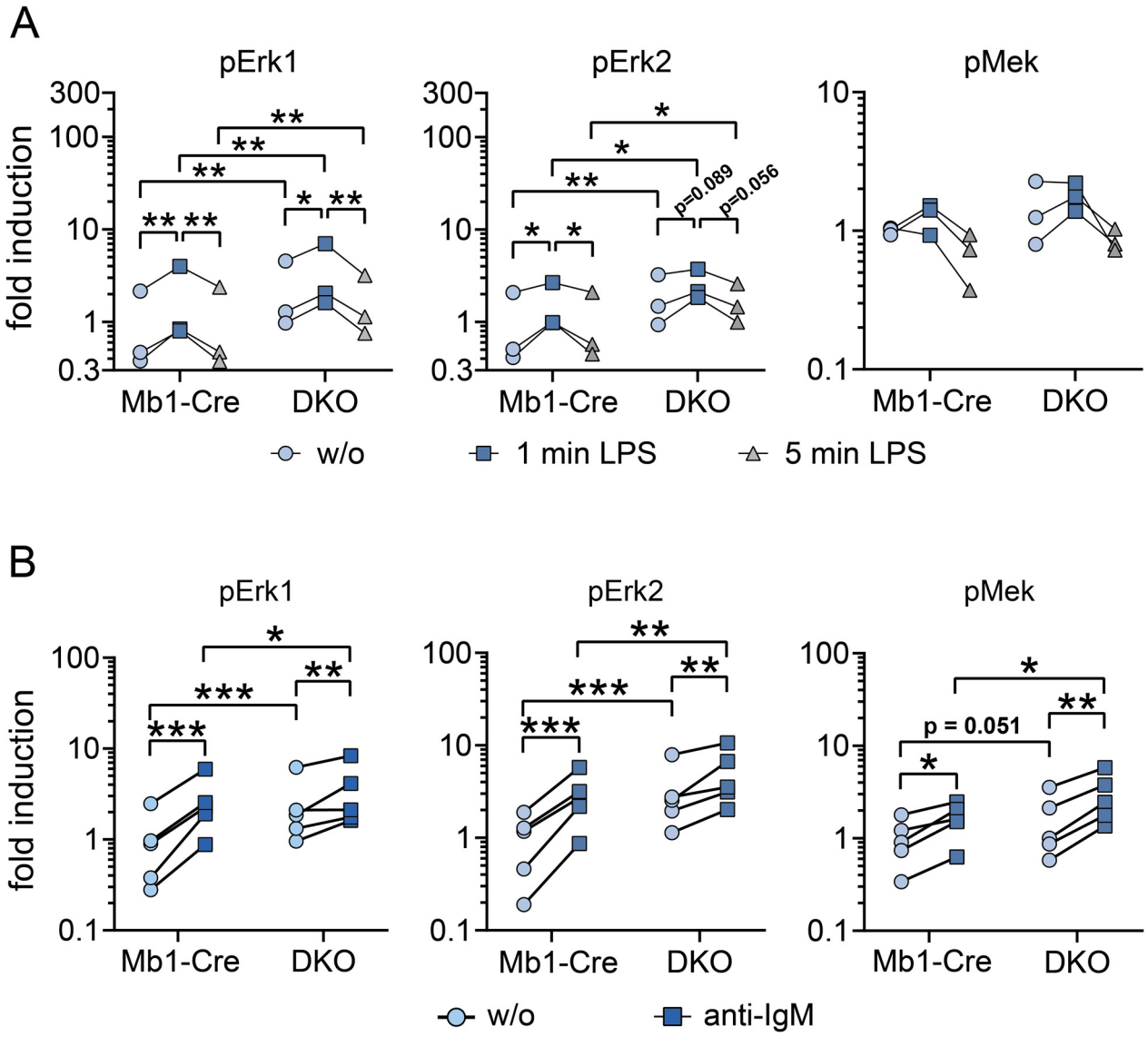

Fig. S6. Abundance of pMEK and pERK in unstimulated and stimulated B cells. (**A** and **B**) Splenic B cells from Mb1-Cre and DKO mice were stimulated for the indicated amonts of time with LPS (**A**) or with an IgM-specific antibody (**B**). The graphs show the fold induction (individual values) of pERK1, pERK2, and pMEK relative to the mean value in unstimulated B cells from Mb1-Cre mice. *N* = 3 (A) and *N* = 5 (B) independent samples per condition and genotype. The values were logarithmic transformed due to their lognormal distribution. Statistics was calculated with 2way RM ANOVA with Tukey's multiple comparison. * P<0.05, ** P<0.01, *** P<0.001.

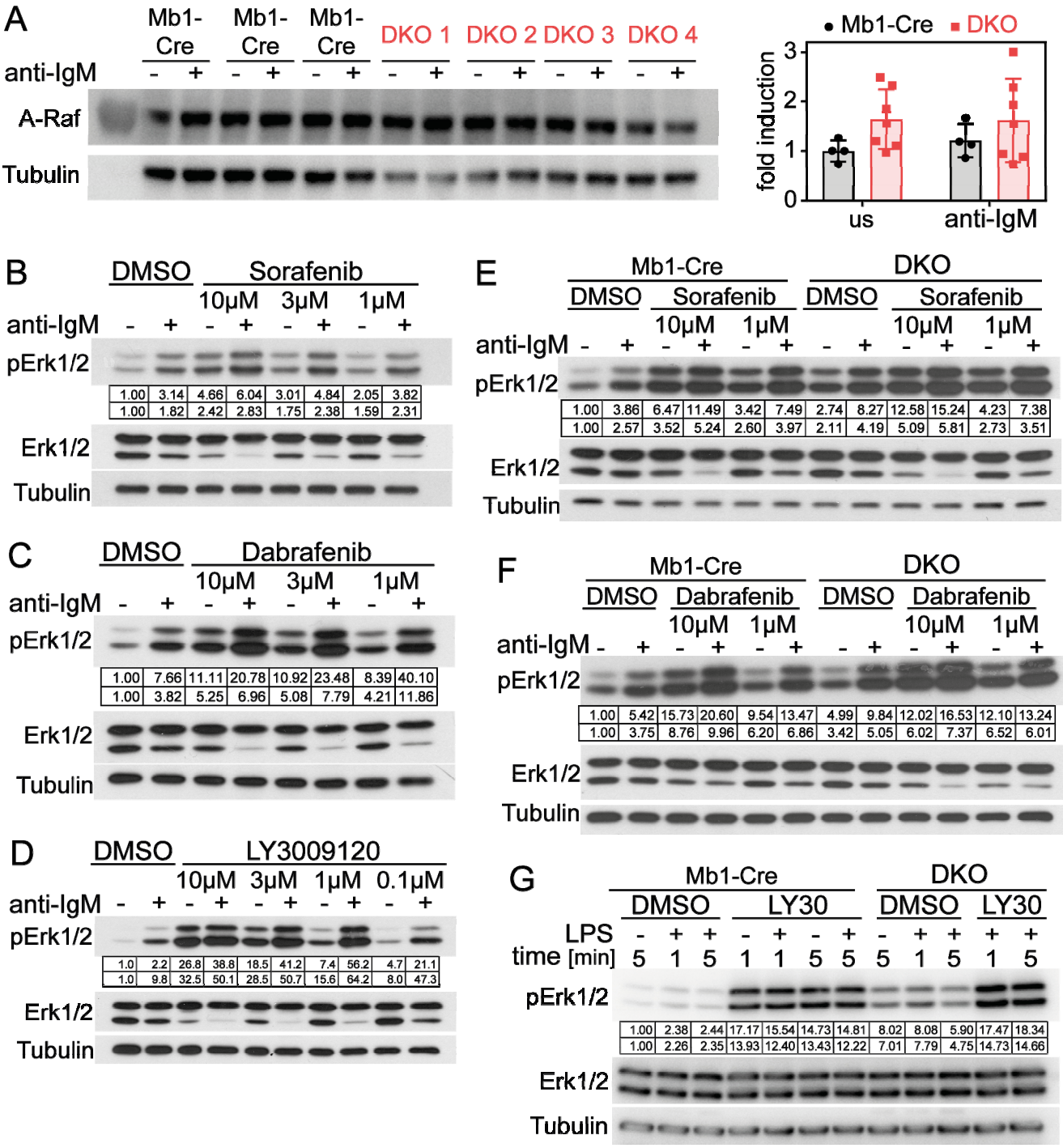
A
Mb1-Cre
Mb1-Cre
Mb1-Cre
DKO 1
DKO 2
DKO 3
DKO 4
anti-IgM
A-Raf
Tubulin
Mb1-Cre
DKO
fold induction
us
anti-IgM
B
DMSO
Sorafenib
10μM
3μM
1μM
anti-IgM
pErk1/2
1.00 3.14 4.66 6.04 3.01 4.84 2.05 3.82
1.00 1.82 2.42 2.83 1.75 2.38 1.59 2.31
Erk1/2
Tubulin
C
DMSO
Dabrafenib
10μM
3μM
1μM
anti-IgM
pErk1/2
1.00 7.66 11.11 20.78 10.92 23.48 8.39 40.10
1.00 3.82 5.25 6.96 5.08 7.79 4.21 11.86
Erk1/2
Tubulin
D
DMSO
LY3009120
10μM
3μM
1μM
0.1μM
anti-IgM
pErk1/2
1.0 2.2 26.8 38.8 18.5 41.2 7.4 56.2 4.7 21.1
1.0 9.8 32.5 50.1 28.5 50.7 15.6 64.2 8.0 47.3
Erk1/2
Tubulin
E
Mb1-Cre
DKO
DMSO
Sorafenib
DMSO
Sorafenib
10μM
1μM
10μM
1μM
anti-IgM
pErk1/2
1.00 3.86 6.47 11.49 3.42 7.49 2.74 8.27 12.58 15.24 4.23 7.38
1.00 2.57 3.52 5.24 2.60 3.97 2.11 4.19 5.09 5.81 2.73 3.51
Erk1/2
Tubulin
F
Mb1-Cre
DKO
DMSO
Dabrafenib
DMSO
Dabrafenib
10μM
1μM
10μM
1μM
anti-IgM
pErk1/2
1.00 5.42 15.73 20.60 9.54 13.47 4.99 9.84 12.02 16.53 12.10 13.24
1.00 3.75 8.76 9.96 6.20 6.86 3.42 5.05 6.02 7.37 6.52 6.01
Erk1/2
Tubulin
G
Mb1-Cre
DKO
DMSO
LY30
DMSO
LY30
LPS
time [min]
5 1 5 1 1 5 5 5 1 5 1 5
pErk1/2
1.00 2.38 2.44 17.17 15.54 14.73 14.81 8.02 8.08 5.90 17.47 18.34
1.00 2.26 2.35 13.93 12.40 13.43 12.22 7.01 7.79 4.75 14.73 14.66
Erk1/2
Tubulin

Fig. S7. ERK phosphorylation in the presence of pan-RAF inhibitors. (**A**) Western blot analysis of A-Raf in lysates from unstimulated and IgM-stimulated splenic B cells from DKO and Mb1-Cre mice. The graph compiles the quantified A-Raf signals. Symbols represent values from individual mice. Means ±SD of the fold induction of A-Raf relative to the mean of the unstimulated controls are shown. Data are representative for $N = 4$ Mb1-Cre and $N = 7$ DKO mice. Two-way ANOVA with Tukey´s multiple comparison test. (**B to F**) Western blot analyses for pERK, ERK1/2, and Tubulin in lysates from splenic B cells isolated from WT (B to D) or Mb1-Cre and DKO B cells (E and F) treated with the indicated concentrations of the pan-RAF inhibitors Sorafenib (B and E), Dabrafenib (C and F), or LY3009120 (D) and stimulated or not with an IgM-specific antibody as indicated. DMSO is a vehicle control. (B to D) $N = 2$ independent sample preparations, each treated with three different inhibitor concentrations. (E) $N = 3$ independent sample preparations for controls, each treated with two different inhibitor concentrations and $N = 2$ for DKO. (F) $N = 3$ independent sample preparations for controls, $N = 1$ for DKO, each treated with two different inhibitor concentrations. **(G)** Immunoblotting for pERK, ERK1/2, and Tubulin in lysates from splenic B cells isolated from Mb1-Cre or DKO mice. B cells were stimulated for the indicated amonts of time with LPS in the presence or absence of the pan-RAF inhibitor LY3009120. Data of the blot are representative for $N = 3$ independent samples per genotype and condition. (B to G) Numbers below the pERK blots show the amounts of pErk1 and pErk2 relative to the unstimulated and uninhibited values (set to 1) after normalization to Tubulin.

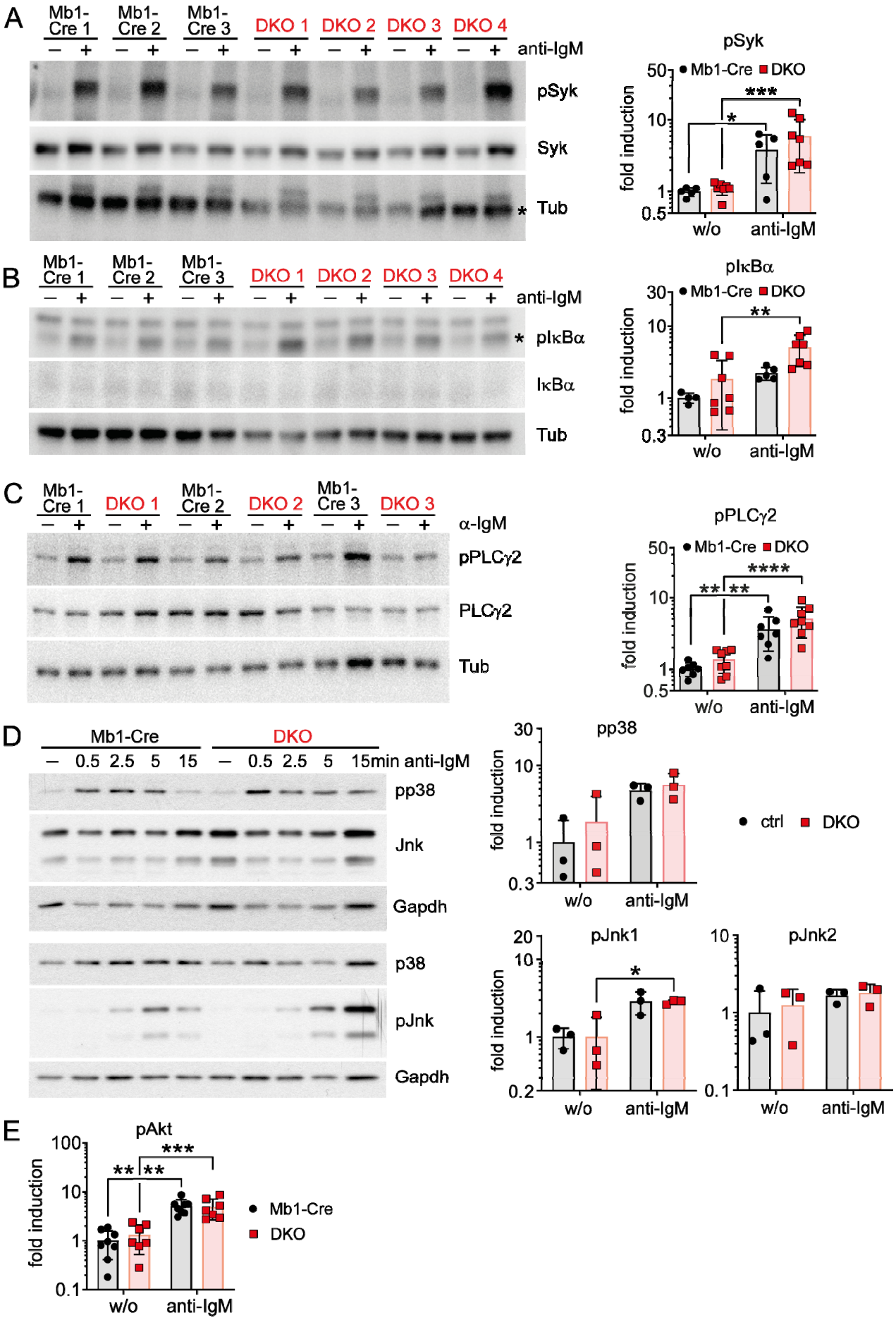
A
Mb1-Cre 1
Mb1-Cre 2
Mb1-Cre 3
DKO 1
DKO 2
DKO 3
DKO 4
anti-IgM
pSyk
Syk
Tub
pSyk
Mb1-Cre
DKO
fold induction
w/o
anti-IgM
B
pIκBα
IκBα
Tub
C
α-IgM
pPLCγ2
PLCγ2
Tub
D
Mb1-Cre
DKO
0.5 2.5 5 15 0.5 2.5 5 15min anti-IgM
pp38
Jnk
Gapdh
p38
pJnk
ctrl
pJnk1
pJnk2
E
pAkt

Fig. S8. Activation of signaling pathways downstream of the BCR. (**A to E**) Western blot analyses and quantification of the indicated signaling molecules that are activated downstream of the BCR in lysates from splenic B cells isolated from control and DKO mice and either stimulated or not with an IgM-specific antibody for 2.5min (A, B, C, and E) or for the indicated amounts of time (D). The experiments shown in (A, B, C, E) are representative for $N = 4$-7 individual samples from Mb1-Cre and $N = 7$-8 from DKO mice. (D) Data are representative for $N = 3$ indipendent samples per genotype and condition. For the quantification of pp38 and pJNK the values after 2.5min anti-IgM stimulation were used. (A to E) Mean±SD of the fold induction of the phosphorylated forms of the indicated signaling molecules in comparison to the mean of unstimulated (w/o) controls (set to 1) are shown. All values were logarithmic transformed due to their lognormal distribution. Two-way ANOVA with Tukey´s multiple comparison test. * P<0.05, ** P<0.01, *** P<0.001, **** P<0.0001. .XXXXXXX.

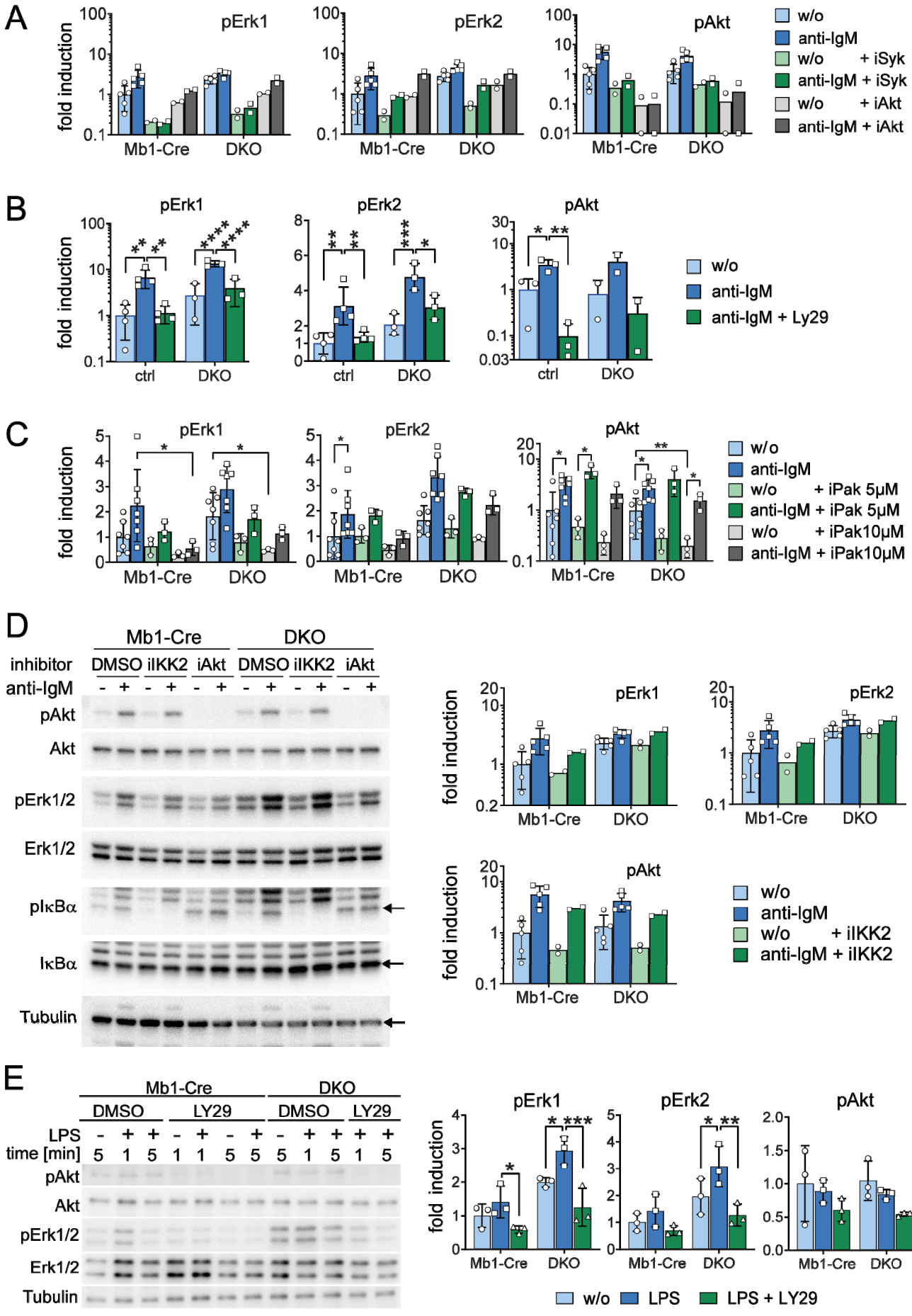
A
pErk1
pErk2
pAkt
fold induction
Mb1-Cre
DKO
w/o
anti-IgM
w/o + iSyk
anti-IgM + iSyk
w/o + iAkt
anti-IgM + iAkt
B
pErk1
pErk2
pAkt
fold induction
ctrl
DKO
w/o
anti-IgM
anti-IgM + Ly29
C
pErk1
pErk2
pAkt
fold induction
Mb1-Cre
DKO
w/o
anti-IgM
w/o + iPak 5μM
anti-IgM + iPak 5μM
w/o + iPak10μM
anti-IgM + iPak10μM
D
Mb1-Cre
DKO
inhibitor
DMSO
iIKK2
iAkt
anti-IgM
pAkt
Akt
pErk1/2
Erk1/2
pIκBα
IκBα
Tubulin
fold induction
pErk1
pErk2
pAkt
Mb1-Cre
DKO
w/o
anti-IgM
w/o + iIKK2
anti-IgM + iIKK2
E
Mb1-Cre
DKO
DMSO
LY29
LPS
time [min]
pAkt
Akt
pErk1/2
Erk1/2
Tubulin
fold induction
pErk1
pErk2
pAkt
Mb1-Cre
DKO
w/o
LPS
LPS + LY29

Fig. S9. RAF-independent ERK phosphorylation in mature B cells. Splenic B cells from control and DKO mice were treated with vehicle (DMSO) or chemical inhibitors: LY30 (pan-RAF inhibitor LY3009120), iSYK (SYK inhibitor p505-15), iAKT (AKT inhibitor AKTi-1/2), LY29 (PI3K inhibitor LY294002) iPAK (PAK inhibitor PF-3758309) or iIKK2 (IKK2 inhibitor8). **(A to C)** Quantification of the Western blots from Fig. 7. The graphs depict the fold induction of pAkt, pErk1, and pErk2 of IgM-stimulated B cells in the presence and absence of the indicated chemical inhibitors. The values were calculated in the comparison to the mean of unstimulated (w/o) control B cells, which was set to 1. (A) $N = 2$ independent samples per genotype for iSyk and iAkt. The graph shows the quantification of the Western-Blots without statistical calculation. (B and C) $N = 3$ independent samples per genotype and condition; Statistics was calculated with two-way ANOVA with Dunnett´s (B) and Sidak´s (C) multiple comparison. * P<0.05, ** P<0.01, *** P<0.001, **** P<0.0001. **(D)** Western blots for the detection of the indicated proteins were performed on lysates from splenic B cells treated with iIKK2 or iAKT and stimulated with an antibody specific for IgM or left unstimulated. The blot is representative for $N = 2$ independent samples per genotype for iIKK2 and iAkt. The graphs show the quantification of the Western blots, without statistical calculation. **(E)** B cells were treated with either DMSO or the PI3K inhibitor LY294002 and then left unstimulated or were stimulated with LPS for the indicated amonts of time. pAKT, AKT, pERK, ERK, and Tubulin were detected by immunoblotting. Western blots were quantified and the fold induction (Mean±SD) of pAkt, pErk1 and pErk2 was calculated in comparison to the mean of unstimulated (w/o) control B cells (set to 1). $N = 3$ independent samples per genotype and condition. (A to E) Two-way ANOVA with Dunnetts´s multiple comparison. * P<0.05, ** P<0.01, *** P<0.001. The values from (C and D) were logarithmic transformed due to their lognormal distribution.

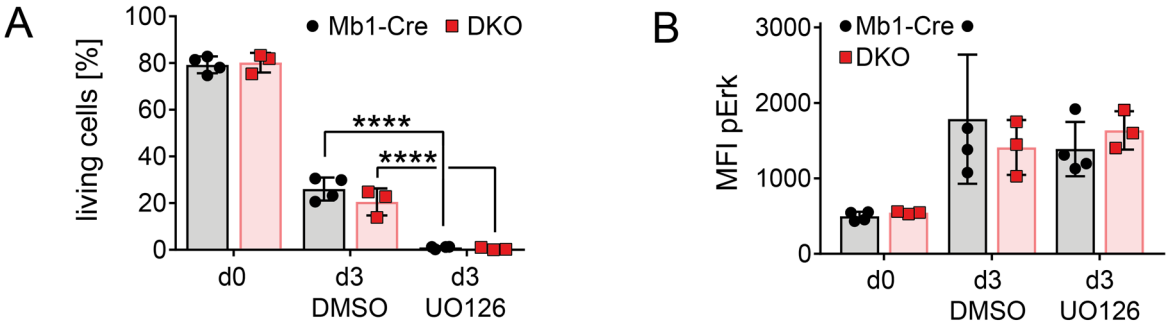

Fig. S10. Survival of B cells in the presence of the MEK inhibitor UO126. Splenic B cells, isolated from DKO or Mb1-Cre mice, were stimulated with LPS in the presence of DMSO or UO126. At day 0 and day 3 the survival of B cells was determined by staining the cells with LIVE/DEAD™. Both the percentages of living cells and MFI for pERK were determined by FACS after permeabilization and intracellular staining. Data are from $N = 3$ independent experiments . Mean±SD are shown. The symbols indicate values of individual mice. [(A) and (B)] Two-way ANOVA with Tukey´s multiple comparison. **** P<0.0001.

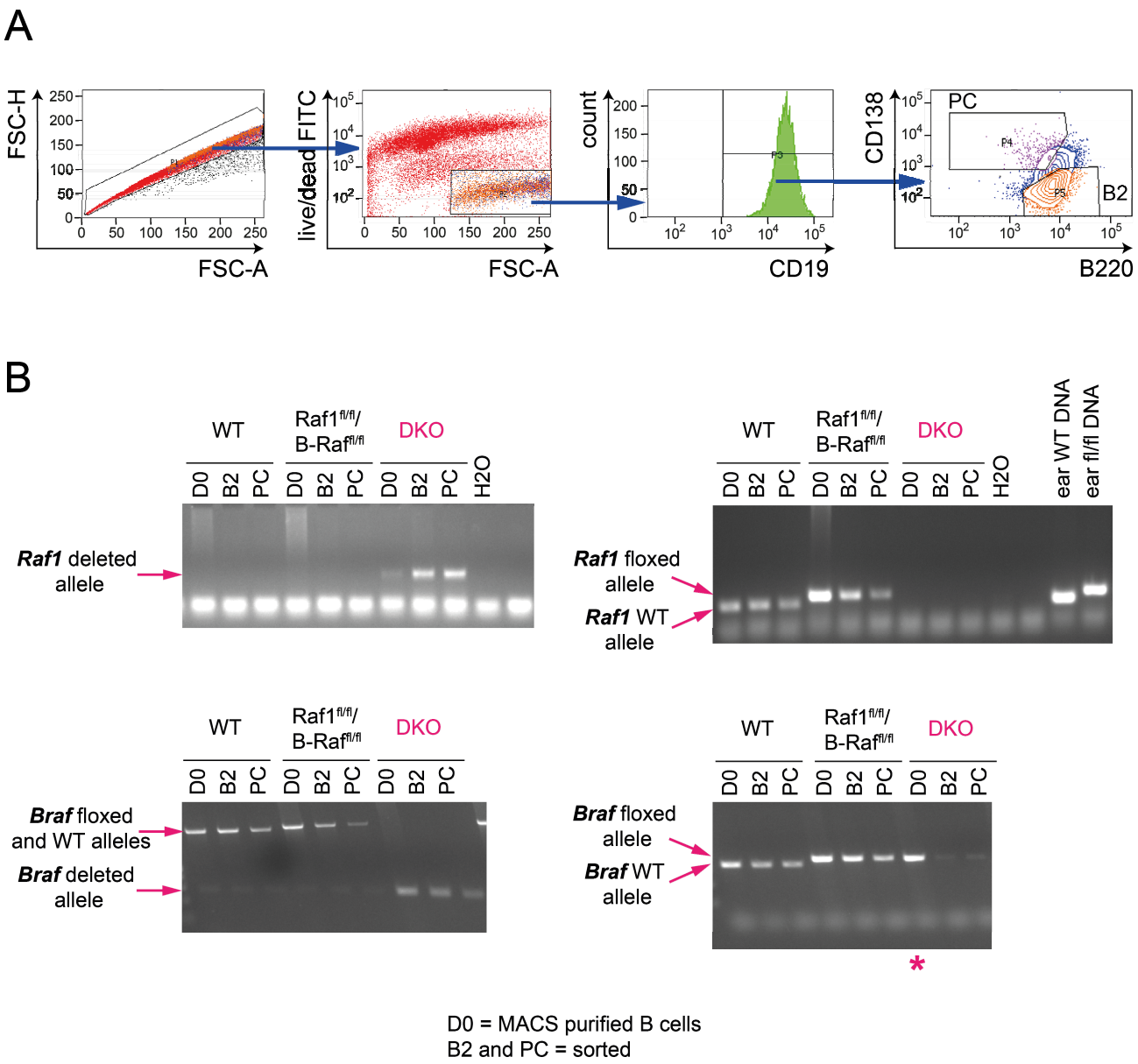

Fig. S11. Deletion of the floxed exons in PCs. (A) Sorting strategy of PC ($CD138^{high}B220^{low}$) and non-PC cells (B2 cells) ($CD138^{low}B220^{high}$). The consecutive gating is indicated in the FACS plots. **(B)** The loxP-flanked regions were amplified by PCR on DNAs prepared from splenic B cells, which were either CD43-depleted (MACS purified d0) or sorted as indicated in (A). The expected fragments are indicated: wild-type locus (wt), recombinant floxed alleles, recombinant deleted alleles. The fragment sizes are indicated in fig. S1, except the undeleted *Braf* floxed and WT alleles, which have a size of around 1.3kb. *The PCR band is due to a low purity of MACS-purified B cells (85%). The PCR is representative of two independent experiments.

Table S1. Antibodies used in this study

	Antibody	Conjugate	Clone	Company	Dilution
FACS	CD43	Biotin; BV421	S7	BD Biosciences	1:100
	SA-APC			BD Biosciences	1:400
	SA-PerCP			BD Biosciences	1:100
	B220	PerCP	RA3-6B2	BD Biosciences	1:400
	BP-1	PE	BP-1	BD Biosciences	1:50
	CD24	FITC	M1/69	BD Biosciences	1:1000
	CD21	APC	7G6	BD Biosciences	1:100
	CD23	PE; FITC	B3B4	BD Biosciences	1:200
	CD5	APC	53-7.3	BD Biosciences	1:500
	IgM	APC	II/41	BD Biosciences	1:100
	AA4.1	PE		eBioscience™	1:200
	PNA	FITC		VectorLaboratories	1:500
	CD95	PE	JO2	BD Biosciences	1:75
	CD138	PE; BV421	281-2	BD Biosciences	1:600; 1:200
	Blimp1	AlexaFluor 647	5E7	BD Biosciences	1:100
	Pax5	PE	1H9	BD Biosciences	1:2000
	Irf4	APC	3E4	BD Biosciences	1:200
	Phospho-Erk1/2 (Thr202/Tyr204)			Cell signaling (#9101S)	1:100
	Rabbit mAb IgG XP Isotype Control		DA1E	Cell signaling (#3900S)	1:100
	goat-anti-rabbit	AlexaFluor 488; PE		invitrogen	1:100
	IgD	FITC	11-26c.2a	BD Biosciences	1:500; 1:200
	CD25	PE	PC61	BD Biosciences	1:400
ELISpot	rat-anti-mouse IgM		R6-60.2	BD Biosciences	1:500
	rat-anti-mouse IgG1		A85-1	BD Biosciences	1:500
	rat-anti-mouse IgG3		R40-82	BD Biosciences	1:500
	rat-anti-mouse IgA		C10-1	BD Biosciences	1:350
	Avidin D - HRP			Vector	1:2000
ELISA	rat-anti-mouse IgG2a		R19-15	BD Biosciences	1:300
	rat-anti-mouse IgA		C10-1	BD Biosciences	1:300
	rat-anti-mouse IgG1		A85-1	BD Biosciences	1:500
	goat-anti-mouse-IgM-HRP		YF97	Southern Biotech	1:5000
	rat-anti-mouse IgG3		R40-82	BD Biosciences	1:500
	Avidin D - HRP			Vector	1:2000
Western blot	Phospho-Erk1/2 (Thr202/Tyr204)			Cell signaling (#9101S)	1:2500
	Erk1/2			Cell signaling (#9102S)	1:2500
	alpha/beta-Tubulin			Cell signaling (#2148S)	1:2500
	Phospho-Akt (Ser473) XP		D9E	Cell signaling (#4060S)	1:2500
	Akt			Cell signaling (#9272S)	1:2500
	Phospho-Mek (Ser217/221)		41G9	Cell signaling (#9154S)	1:1000
	Mek		47E6	Cell signaling (#9126S)	1:1000
	Phsopho-Syk (Tyr525/526)			Cell signaling (#2711S)	1:1000
	Syk			Cell signaling (#2712)	1:1000
	Phospho-p38 MAPK (Thr180/Tyr182) XP		D3F9	Cell signaling (#4511S)	1:1000
	p38 MAPK			Cell signaling (#9212S)	1:1000
	Phospho-IkBalpha (Ser32/36)		5A5	Cell signaling (#9246S)	1:1000
	IkBalpha		44D4	Cell signaling (#4812S)	1:1000
	PLCgamma2			Cell signaling (#3872)	1:1000
	Phospho-PLC-gamma-2 (Tyr1217)			Cell signaling (#3871S)	1:1000
	Phospho-SAPK/JNK (T183/Y185)		81E11	Cell signaling (#4668S)	1:1000
	SAPK/JNK			Cell signaling (#9252L)	1:1000
	GAPDH		6C5	Merck (#CB1001-500UG)	1:20000
	A-Raf			Cell signaling (#4432S)	1:1000
	B-Raf		C19	Santa Cruz Biotechnology	1:500
	Raf-1 (C-Raf)			Cell signaling (#9422S)	1:1000
	Anti-mouse IgG	HRP-linked		Cell signaling (#7076S)	1:2500
	Anti-rabbit IgG	HRP-linked		Cell signaling (#7074S)	1:2500
WES	LaminB2		E1S1Q	Cell signaling (#13823S)	1:50
	Phospho-Erk1/2 (Thr202/Tyr204)			Cell signaling (#9101S)	1:20
Histo	Anti-Mouse IgM (µ-chain specific)	Peroxidase		Sigma-Aldrich	1:100
	Rat-anti-mouse CD3			monoclonal CD3 antibody produced in house	1:2
	Rat-anti-mouse MOMA-1			Biomedicals	1:100
	PNA	Biotin		Vector	1:2000
	mouse-anti-Rat IgG2	Biotin		Jackson Laboratories	1:250

Table S2. Primers for PCR amplification of the *Raf*-genes.

Raf-1 US-Lox	TGGCTGTGCCCTTGGAACCTCAGCACC
Raf-1 DS-Lox	AACATGAAGTGGTGTTCTCCGGGCGCC
Raf-1 CT-U	ATGCACTGAAATGAAAACGTGAAGACGACG
B-Raf 9	GCATAGCGCATATGCTCACA
B-Raf 11	CCATGCTCTAACTAGTGCTG
B-Raf 17	GTTGACCTTGAACTTTCTCC